Article / Discoveries

Evolution of CDK1 paralog specializations in a lineage with fast developing planktonic embryos

Xiaofei Ma[1], Jan Inge Øvrebø[1,2#], Eric M Thompson[1,2 *]

[1]Sars International Centre, and [2]Dept. of Biological Sciences, University of Bergen, Bergen, Norway

[#]Present address: Huntsman Cancer Institute, University of Utah, USA

*Correspondence to: Eric.Thompson@uib.no, ORCID 0000-0002-3756-9036

Running Title: Evolution of CDK1 paralog specializations

Abbreviations: CDK, Cyclin Dependent Kinase; DoS, Determinant of Specificity; RNAi, RNA interference; NEBD, Nuclear Envelope Breakdown;

Key words: PSTAIRE helix; Cyclin B; Tunicate; Coenocyst; Oogenesis; Embryogenesis; Meiosis; X-linkage; Gene duplication

Abstract

The active site of the essential, eukaryotic CDK1 kinase is generated by core structural elements, among which the PSTAIRE motif in the critical αC-helix, is universally conserved in metazoans. The CDK2 kinase, sharing the PSTAIRE, arose early in metazoan evolution and permitted subdivision of tasks along the S-M-phase axis. The marine chordate, *Oikopleura dioica*, is the only metazoan known to possess more than a single CDK1 ortholog, and all of its 5 paralogs show sequence divergences in the PSTAIRE. Through assessing CDK1 gene duplications in the appendicularian lineage, we show that the CDK1 activation loop substrate binding platform, ATP entrance site, hinge region, and main Cyclin binding interface, have all diversified under positive selection. Three of the 5 CDK1 paralogs are required for embryonic divisions and knockdown phenotypes illustrate further subdivision of functions along the S-M-phase axis. In parallel to CDK1 gene duplications, there has also been amplification in the Cyclin B complement. Among these, the CDK1d:Cyclin Ba pairing is required for oogenic meiosis and early embryogenesis and shows evidence of coevolution of an exclusive interaction. In an intriguing twist on the general rule that Cyclin B oscillations on a background of stable CDK1 levels regulate M-phase MPF activity, it is CDK1d protein levels that oscillate, rather than Cyclin Ba levels, to drive rapid, early embryonic cell cycles. Strikingly, the modified PSTAIRE of odCDK1d shows convergence over great evolutionary distance with plant CDKB, and in both *O. dioica*, and plants, these variants exhibit increased specialization to M-phase.

Introduction

The complexity of the eukaryotic cell and its larger genome necessitates greater control over the organization of events during cellular division than for prokaryotic life. The eukaryotic protein kinase, CDK1, whose activity depends on unstable Cyclin regulatory subunits, has key roles in orderly triggering S and M phases from yeast to mammals (Santamaria et al. 2007), by sequential, regulatory phosphorylation of hundreds of substrate proteins. CDK activity levels progressively surpass response thresholds, to trigger serial events in S and M phases (Swaffer et al. 2016). Quantitative changes in CDK activity function as a coarse organizing mechanism for cell cycle transitions, with lower CDK activity resulting in higher affinity S-phase substrate phosphorylation, to carry out DNA replication, and higher activity driving mitotic entry via the phosphorylation of lower affinity mitotic substrates. CDK1 protein levels are constant during the cell cycle (Arooz et al. 2000), and are activated at each phase of the cell cycle by binding of stage-specific cyclins. The intrinsic activity of Cyclin–CDK1 complexes increases in correlation with the appearance of particular cyclins in the cell cycle (Ord and Loog 2019). G1/S cyclins generate CDK complexes with the lowest activity, which manifests in the lowest affinities (k_m) and the lowest catalytic activities (k_{cat}) toward substrates, whereas S-, G2-, and M-phase Cyclins form CDK complexes with higher

57 affinities and catalytic activities towards substrates. The lower CDK activities generated by S- versus
58 M-phase Cyclins also means that S-phase Cyclins do not achieve sufficient CDK1 activity levels to
59 initiate mitosis, helping to ensure resolution of S- and M-phases. Compared to single-celled yeast,
60 metazoans have also evolved CDK2, with lower intrinsic activity than CDK1 in the regulation of S-
61 phase (Ord et al. 2019). Although metazoan CDK1 has become more specialized to M-phase
62 functions it still retains indispensable, ancestral, late S-phase functions (Katsuno et al. 2009; Farrell
63 et al. 2012; Seller and O'Farell 2018; Szmyd et al. 2019).
64 In addition to modulating CDK activity, the Cyclins are also implicated in specifying CDK
65 substrate targets. Cyclins bind different substrate docking motifs: RxF for S Cyclins and LxF for
66 budding yeast M Cyclins, and these Cyclin docking pockets increase specificity to target subsets to
67 further fine-tune the CDK threshold ladder (Koivomagi et al. 2011; Ord et al. 2019). Most CDK
68 substrates contain multiple target sites clustered in disordered regions (Holt et al. 2009), and
69 phosphorylation cascades along these sites are shaped by precisely oriented docking interactions
70 mediated by Cks1, the phospho-adaptor subunit of Cdk1 (Koivomagi et al. 2011). Distances between
71 phosphorylation sites and docking sites are critical for both Cyclin and Cks docking. The composition
72 of phosphorylation sites with respect to serine versus threonine, and surrounding residues, combined
73 with positioning of Cyclin and Cks docking motifs, creates a unique barcode on each substrate. The
74 Cyclin−CDK−Cks1 complexes read the barcodes and assign execution of CDK-triggered switches
75 to specified time points during the cell cycle (Ord et al. 2019).
76 Canonical cell cycle regulation can be modified during development and growth. This is true of
77 rapid mitotic cell cycles observed during early embryogenesis in a wide range of phyla and in the
78 promotion of growth through endocycles in a number of organisms (Edgar and Orr-Weaver
79 2011). Externally developing, nutrient-rich, non-feeding, embryos are at risk of predation, and rapid
80 development is a means of mitigating this risk (Strathmann et al. 2002). Many marine planktonic
81 larvae also continue fast development to first swimming in order to enhance survival (Staver and
82 Strathmann 2002). The pelagic, tunicate, *Oikopleura dioica*, exhibits very rapid embryonic and larval
83 development, undergoing metamorphosis to a feeding juvenile within 12 h at 15 °C (Bouquet et al.
84 2009). Very rapid growth and extensive modulation of reproductive output over several orders of
85 magnitude are then achieved through deployment of a variety of endoreduplicative cell cycle variants
86 (Ganot and Thompson 2002; Ganot et al. 2007). These adaptations allow the organism to rapidly
87 adjust population levels in response to algal blooms, during an extremely short chordate life cycle (6
88 days at 15 °C). Accompanying this life history strategy is considerable modification of the
89 organism's molecular cell cycle regulatory complement (Campsteijin et al. 2012), including gene
90 duplications to generate multiple CDK1 and Cyclin B paralogs.
91 All metazoans examined to date possess a single CDK1 ortholog that exhibits a highly conserved
92 PSTAIRE motif in the critical αC-helix structural element located within the N-lobe of CDK1 and
93 CDK2. This element is an important interface in docking interactions with Cyclin partners and in

contributing to formation of the kinase active site (Wood et al. 2019). *O. dioica*, aligns with other metazoans in possessing a CDK2 with a conserved PSTAIRE motif, but deviates distinctively in that it has evolved 5 CDK1 paralogs, all of which show deviations in the critical PSTAIRE motif. Here, we have examined how these paralogs have arisen in the appendicularian lineage and to what extent they exhibit functional specializations along the CDK2-CDK1, S- to M-phase, cell cycle, regulatory axis. We show that the CDK1 substrate binding platform, activation loop, ATP entrance site, hinge region, and the main Cyclin binding interface, have all diversified under positive selection. In meiosis and early embryogenesis, CDK1 paralogs were sequentially activated across the cell cycle. Combinatorial knockdowns revealed collaboration of CDK2, CDK1a, CDK1b and CDK1d along the S- to M-phase axis in oogenic meiosis and early embryonic divisions. Interestingly, the Cyclin Ba and CDK1d paralogs are located in proximity on the recently evolved *O. dioica* X chromosome, were co-expressed specifically during oogenic meiosis and early embryogenesis, and were required for these processes. Modifications of critical residues in the Cyclin B:CDK1 interface and the salt bridge, suggest that CDK1d and Cyclin Ba may have coevolved an exclusive interaction that does not interfere with the more canonical CDK1a/b/c:CycBc interactions in regulating M-phases during early developmental events. It is generally universal in metazoan mitotic cycles that CDK1 protein levels remain relatively constant throughout the cell cycle whereas Cyclin B levels oscillate and are up-regulated during M-phase. In contrast, we reveal a novel regulatory oscillation of levels of the CDK1d paralog, as opposed to its Cyclin Ba interacting partner, that drive early, very rapid embryonic cell cycles in this planktonic chordate.

Results

Episodic positive selection of CDK1 orthologs after duplication

Metazoans possess a single CDK1, with the exception of *Oikopleura dioica*, where 5 CDK1 paralogs have been identified (Campstejin et al. 2012). To trace the origins of this amplification we analyzed genomes and transcriptomes of five appendicularian species in the *Oikopleura* and *Fritillaria* genera (Naville et al. 2019). *CDK1a, b and c* were uniformly present, whereas *CDK1d* and *e* appear to have arisen from *CDK1c* specifically in *O. dioica,* the only known dioecious appendicularian (fig. 1A). Interspecies clustering of *CDK1* paralogs and interspecies conservation of their intron-exon structures (supplementary fig. S1) suggest that *CDK1* amplification arose through early DNA-based duplication events in the *Oikopleura* lineage. Based on phylogenetic analyses, *CDK1a* duplication gave rise to *CDK1b* that was subsequently duplicated to generate *CDK1c,* which then gave rise to the *O. dioica* specific*, odCDK1d*. This duplication gradient pattern, and young paralogs-biased duplication, have not previously been reported in metazoans. *O. albicans CDK1a*, *b* and *c* locate on the same chromosome. *O. dioica CDK1a* and *b* locate on the same autosome whereas *CDK1c* is present on a different autosome that also contains *CDK1e* (fig. 1C). *CDK1d* is found on the X

130 chromosome where, at a distance of 5 MB, the *CycBa* locus is also located. Following the
131 classification system for paralog subtypes (Sonnhammer and Koonin 2002), *Oikopleura* genes in the
132 *CDK1a* clade are orthologs, and *odCDK1a* and *b* are outparalogs to each other when comparing *O.*
133 *dioica* with *O. albicans*, since CDK1 duplication happened before *O. dioica* and *O. albicans*
134 speciation. *O. dioica CDK1c, d* and *e* are inparalogs to each other when comparing *O. dioica* with
135 *O. albicans,* since CDK1c duplication happened after *O. dioica* and *O. albicans* speciation.
136 Both the new Nei-Gojobori method (Zhang et al. 1998) and Codon-based models (Yang 2007)
137 were applied to analysis of *Oikopleura* CDK1s. During the 3 rounds of gene duplication, the lineage
138 subtending *CDK1a* (fig. 1A) experienced positive selection (bn/bs = 2.48, P=0.0386, dN/dS(ω) =
139 41.01, p = 0.081, P = 0.0481), as did *CDK1b* (bn/bs = 4.72, P = 0.0305, dN/dS(ω) = 28.14, p = 0.046,
140 P = 0.003) and *CDK1c* (bn/bs = infinite, P = 0.033, dN/dS(ω) = 999, p = 0.066, P=0.002) (fig. 1A,
141 supplementary table S1). To better understand positively selected sites identified by Codon-based
142 models, we aligned CDK1 sequences from 15 metazoan phyla, and Cdc28 from budding yeast. Sites
143 conserved in metazoan sequences, but substituted in *Oikopleura* CDK1 orthologs, were mapped to
144 human CDK1 and CDK2 crystal structures (supplementary figs. S2 and S3). Determinants of kinase
145 specificities (DoS) (Creixell et al. 2015) were aligned and the DoS that are conserved in metazoan
146 CDK1 orthologs but substituted in *Oikopleura* CDK1 sequences were mapped to human CDK1-
147 Cyclin B1 crystal structures. During kinase evolution, the critical catalytic residues, regulatory
148 hydrophobic spine and catalytic hydrophobic spine have been conserved. The diversification of the
149 substrate binding platform-activation segment, and indirect ATP binding sites, drive diversification
150 of substrate specificity and substrate phosphorylation efficiency. *Oikopleura* CDK1s have the same
151 active site as human *CDK1* and yeast cdc28, including the Mg^{2+}-binding loop (DFG), important
152 residues in the catalytic loop, the catalytic hydrophobic spine, the regulatory hydrophobic spine and
153 the salt bridge (Wood et al. 2019) (supplementary figs. S2 and S3). The bn/bs values below 1,
154 observed among CDK1 sequences (fig. 1A), suggest that these orthologs are functional kinases under
155 purifying selection. Conservation in the DFG+1 residues (Leu) in the 17 *Oikopleura* CDK1
156 sequences, suggests that they share with human CDK1, a preference for serine over threonine as a
157 phosphor-acceptor residue in substrates (Chen et al. 2014). However, the ATP binding sites, substrate
158 binding sites and Cyclin binding interfaces have diversified in *Oikopleura* CDK1 paralogs.

159 **Substitutions in ATP binding sites**

160 In the protein kinase family, the ATP binding site is very conserved, but adjacent areas not occupied
161 by ATP are more variable, particularly in the hinge region (E81-K89, human CDK1 numbering).
162 These sites modulate ATP affinity. This region may determine the different catalytic efficiencies of
163 CDK1 and CDK2, as substitutions in the hinge of CDK2, that mimic amino acids in this region of
164 CDK1 (substitute N84, Q85 in CDK2 to 84S, 85M in CDK1), increase both ATP affinity (k_m ATP)
165 and turn over (k_{cat}) (Echalier et al. 2012). In the opposite direction, a K89D/E mutation in the CDK2

166 sequence, reduces k_{cat}. *Oikopleura* CDK1 paralogs have diversified in the hinge region. CDK1c
167 paralogs exhibit an S84F/Y substitution whereas this site is conserved in CDK1a paralogs compared
168 to the metazoan consensus (supplementary fig. S2). The M85 site is a DoS, and a M85C substitution
169 occurred in CDK1a of *O. vanhoeffeni*, *O. albicans* and *O. dioica*, after they split from *O. longicauda.*
170 This substitution has been positively selected (supplementary table S1), possibly driving
171 diversification of ATP affinity among CDK1 paralogs following their duplication. *Oikopleura*
172 CDK1a and b orthologs have substitutions at K89, a residue that is conserved in CDK1 and CDK2
173 from yeast to metazoans (supplementary fig. S2). This raises the possibility that CDK1a and b may
174 have lower ATP affinity and substrate phosphorylation efficiency compared to CDK1c, d and e
175 paralogs. Indeed, as shown later, we found that CDK1d peaks in M phase whereas CDK1a was
176 present earlier in interphase. The CDK1 L83 residue is also conserved form yeast to human, with the
177 amide of L83 forming a hydrogen bond with the heteroaromatic adenine ring of ATP (Bao et al.
178 2011). This residue is conserved in CDK1a and c, but has been modified to L83M in the hinge region
179 of all *Oikopleura* CDK1b orthologs. Thus, CDK1 paralogs have different signatures in their hinge
180 regions, suggesting diversification in their ATP affinities and catalytic efficiencies.
181 The conserved DoS, P61, is located in the N-lobe, in the loop connecting the PSTAIRE helix and
182 β4 of human CDK1 (supplementary fig. S2). Positive selection of a P61E substitution in all
183 *Oikopleura* CDK1a orthologs, suggests that positive selection occurred after the initial CDK1
184 duplication but prior to speciation. This asymmetric adaptive evolution of an evolutionary conserved
185 DoS in one of the duplicates, and conservation of this substitution within CDK1a orthologs, could
186 be best explained by escape from adaptive conflicts after duplication (Des Marais and Rausher 2008).

187 **Substitution in the activation segment**

188 The activation segment forms an integral part of the substrate binding groove, and diversity in this
189 loop contributes to the wide range of substrate specificities and affinities of protein kinases (Nolen
190 et al. 2004). The structure of CDK1 suggests a mechanism through which activation loop flexibility,
191 embedded in a more flexible CDK1 fold, allows CDK1 to accommodate a more diverse substrate set
192 than CDK2 (Brown et al. 2015). These plastic properties may also contribute to its ability to partner
193 non-cognate cyclins in the absence of other CDKs to drive a complete metazoan cell cycle[1]. In
194 *Oikopleura* CDK1 paralogs, sites in the activation segment that bind to substrate, P0 (L149, T166),
195 P+1 (V164, V165) and P+3 (T161), are the same as in yeast and human CDK1 (supplementary fig.
196 S2). However, several conserved sites in the activation segment have been dramatically modified in
197 *Oikopleura CDK1* paralogs*,* particularly in *O. dioica CDK1c, d* and *e* inparalogs. G154 is located at
198 the tip of the human CDK1 activation segment where it is important in forming the β turn in the short
199 β hairpin structure when CDK1 binds to Cyclin B1 (Brown et al. 2015) (supplementary fig. S3).
200 Human CDK2 cannot form this hairpin structure (Jeffrey et al. 1995), and this is a major difference
201 in the activation segment between CDK1 and CDK2. The G154 site is conserved in yeast and

metazoans, but has diversified in *Oikopleura* CDK1 paralogs. A G154N substitution occurred in *Oikopleura* CDK1a, G154S in *Oikopleura* CDK1b, and G154K in *O. dioica* CDK1c, d and e (supplementary fig. S2). This site is also identified as having experienced positive selection (supplementary table S1), suggesting adaptive diversification of the activation segment by disrupting the β-turn though substitution with large side chain residues. Immediately downstream of this substitution, *O. dioica* CDK1c, d and e all have an I157F substitution, whereas CDK1c paralogs from other *Oikopleura* species have an I157M substitution. *O. dioica* CDK1c, d and e also exhibit substitutions at theV159 and Y160 sites, two residues immediately upstream of the important, regulatory phospho T161 site. The V159 site is also a DoS, conserved from yeast to humans. Finally, in human CDK1, L167 (conserved from yeast to human) is adjacent to the substrate P-2 residue (Brown et al. 1999; Bao et al. 2011) (supplementary fig. S4). The L167M substitution found in all CDK1b and c orthologs, presents a larger side chain, which may affect affinity towards P-2 residues.

Substitutions in the PSTAIRE helix

The CDK1 PSTAIRE helix is invariant in metazoans and yeast. Mutation screens in yeast *cdc28* revealed that the exact PSTAIRE helix sequence (PSTAIREISLLKE) is required for cell division, and any mutations in this domain are lethal (MacNeill and Nurse 1993; Levine et al. 1999; Ahn et al. 2001;). The A48V substitution in cdc2 in *S. pombe* is dominant negative, as the mutant cdc2 could bind Cyclin but could not be activated (Fleig et al. 1992), whereas an A48T substitution in *S. cerevisiae cdc28* inhibits CLB2 association (Ahn et al. 2001). Surprisingly, the PSTAIRE helix is modified in all *Oikopleura* CDK1 paralogs (fig. 1A) whereas *Oikopleura* CDK2s retain the canonical PSTAIRE sequence. All of the 17 identified *Oikopleura* CDK1 sequences share the A48S substitution (supplementary figs. S1 and S2). The S48 residues in *Oikopleura* CDK1 sequences are encoded by two disjoint codon sets, TCN and AGY, which cannot be interconverted by a single nucleotide mutation. Accordingly, switches between serine codons from the two sets can occur either directly, by simultaneous double (tandem) mutation (TC > AG), or indirectly, via two consecutive single-nucleotide substitutions (TC > AC > AG or TC > TG > AG). This is consistent with strong positive selection (Rogozin et al. 2016) at these sites in CDK1 sequences within the entire *Oikopleura* genus. Interestingly, coincident with the A48S substitution, codons for S48 in all CDK1b and c paralogs, except olCDK1c, have phase 2 intron insertions (supplementary fig. S1). This intron insertion is specific to *Oikopleura*, and is not found in any other metazoan CDK1.

O. dioica CDK1b and d (and *O. longicauda* CDK1b) have an additional S46P substitution in the PSTAIRE helix whereas *O. dioica* CDK1c and e have an S46A substitution at this residue. The double proline predicts that the odCDK1b and d PSTAIRE helices would be shorter and exhibit an altered orientation compared to human CDK1. The *O. dioica* CDK1a, b and d versions of the PSTAIRE helix complemented yeast *cdc28* temperature sensitive mutants, whereas *O. dioica* CDK1c and e did not (fig. 1D). *O. dioica* CDK1c, d and e inparalogs also share double S53C and L54T/S

238 substitutions in the PSTAIRE helix (supplementary fig. S2). Human CDK1 S53 forms hydrogen
239 bonds with Cyclin B1 L296 and G297 amide groups (Brown et al. 2015) (located at the C-terminal
240 loop connected to the α5 helix) (supplementary fig. S3). Substituting serine at this site with cysteine
241 may reduce CDK1c inparalog interaction interfaces with Cyclin B.

242 In summary, critical elements for catalysis are conserved in *Oikopleura* CDK1 paralogs, but they
243 diverge in binding sites for ATP and substrates, suggesting qualitative differences in catalysis.
244 Therefore, we set out to determine expression profiles and evaluate knockdowns of *O. dioica* CDK1
245 paralogs to characterize their individual functions in meiosis and early embryonic cell cycles.

246 **Transcription of *CDK1d* and *cycBa* is restricted to oogenesis**

247 *CDK1a, b, c* and *cycBc* are generally present in the *Oikopleura* genus (fig. 1A and B). In *O. dioica*,
248 they were broadly expressed, in a sexually unbiased manner, in embryos, juveniles, and mature
249 animals (fig. 2). In contrast, *CDK1d* and *e,* and *cycBa* are thus far, specific to *O. dioica,* and were
250 transcribed during oogenesis. Their transcripts persisted during early embryogenesis (figs. 2 and 6B).
251 *CycBa* was not expressed in juveniles or testes. Interestingly, *O. dioica CDK1d* has different
252 transcription start sites (TSS) in testes and ovaries. The ovarian *CDK1d* TSS occurs before the ATG
253 start codon located in the first exon. In testis, a sharp TSS located within the first intron yields
254 nonsense transcripts (fig. 1E). Western blots confirmed that the CDK1d protein was present in
255 ovaries but absent in testes (fig. 2B). *CDK1d* mRNAs began to degrade after fertilization and dropped
256 to very low levels at 2.5 h post-fertilization (fig. 6B). Given these differential expression patterns,
257 we then undertook to knockdown the five CDK1 paralogs and 2 Cyclin Bs in *O. dioica* individually,
258 or simultaneously, to explore functions of the expanded CDK1-Cyclin B complement.

259 **CDK1a, b and d collaborate in embryonic divisions: a conserved PSTAIRE is not required**

260 The five odCDK1 paralogs and odCDK2 were each targeted for knockdown by RNAi. After
261 injections of dsRNA in gonads of day 4 or 5 animals, oocytes were collected and processed to verify
262 specific knockdown by RT-qPCR, and western blots. Successfully knocked down oocytes were
263 exposed to wild type sperm and embryonic divisions were examined. Previous reports of CDK1a
264 RNAi at day 4 demonstrated that this impaired vitellogenesis and meiosis resumption (Ovrebo et al.
265 2015; Feng and Thompson, 2018). CDK1a RNAi at day 5 avoided these defects and injected animals
266 produced normal size oocytes. However, embryonic divisions were delayed and they failed to hatch
267 (fig. 3A). When CDK1b was knocked down, embryonic cell cycles were also delayed and embryos
268 arrested at gastrulation, corresponding to 2.5 h post-fertilization of normal embryos (fig. 3B).
269 Knockdown of CDK1d yielded 3 phenotypes: a complete failure to emit polar bodies, arrest after
270 polar body emission, or abnormal divisions after polar body emission (fig. 3C-G). These phenotypes
271 reflect roles of odCDK1d in nuclear envelope breakdown (NEBD) (Ovrebo et al. 2015) and spindle
272 assembly in meiosis I, for meiosis completion (Feng and Thompson 2018), and subsequent mitotic
273 divisions. No significant differences were observed in the proportions of normal hatching embryos

274 between wild type, and any of the *CDK1c, e,* or *c+e* RNAi knockdown embryos (supplementary fig.
275 S5). CDK1c and e have very similar PSTAIRE helices (PATSI/VRE, fig. 1A), they failed to rescue
276 yeast *cdc28* mutants, and they were also dispensable for embryonic divisions.
277 CDK2 is dispensable for early mouse early embryogenesis and mitotic cycles in cultured
278 vertebrate cells (Santamaria et al. 2007). Consistent with these observations, *odCDK2* RNAi embryos
279 divided normally and hatched with correct timing (fig. 4A). CDK2 is the only CDK in *Oikopleura*
280 that has a canonical PSTAIRE helix. This indicates that the exact sequence in the conserved metazoan
281 CDK1, PSTAIRE helix, is not required for *Oikopleura* embryonic divisions. After emission of polar
282 bodies, *CDK1a* + *CDK2* RNAi zygotes arrested prior to pronuclear fusion (fig. 4B). The synergistic
283 defects during the cell cycle caused by *CDK1a+CDK2* RNAi suggests CDK1 and CDK2 have
284 overlapping roles in interphase. Since *CDK2* RNAi embryos divided normally, defects arising from
285 *CDK1a+CDK2* RNAi suggest *CDK1a* could complement CDK2's roles in interphase during
286 embryonic divisions. Immunostaining of tadpoles developed from oocytes injected with *CDK1a-*
287 *GFP* capped mRNA, showed CDK1a located to the nucleus during interphase (supplementary fig.
288 S6). *CDK1a+b* RNAi embryos arrested at the 4th or 5th division at prophase with super-condensed
289 chromosomes closely juxtaposed to the nuclear lamina (fig. 4D). The synergistic defects during the
290 cell cycle cause by *CDK1a+b* RNAi suggests collaborative roles of CDK1a and CDK1b during
291 prophase, the point at which CDK1b localized to chromatin (supplementary fig. S6).

292 **Coevolution of *Oikopleura dioica* CDK1d and Cyclin Ba**

293 Vertebrate Cyclin B1 is required for meiosis and mitosis. Most invertebrates, except *C. elegans* (van
294 der Voet et al. 2009), have a single ortholog of vertebrate Cyclin B1/B2 (fig. 1B), and this ortholog
295 is required for meiosis and mitosis (Okano-Uchida et al. 1998). Oscillation of Cyclin B levels
296 orchestrate CDK1 kinase activity during M-phase. As for other invertebrates, all 4 hermaphroditic
297 *Oikopleura* species have a single Cyclin B (Cyclin Bc), whereas dioecious *O. dioica* has Cyclins Ba
298 and Bb (almost identical to Ba) in addition to Cyclin Bc. The *cycBa* gene is located on the X
299 chromosome, and is specifically expressed in ovaries. Knockdown of Cyclin Bc, showed no
300 significant differences in Cyclin Ba levels, H1 kinase activity in oocytes, or embryonic development
301 compared to wild type (fig. 5A), indicating that Cyclin Bc is dispensable for meiosis and embryonic
302 divisions. In contrast, *cycBa* RNAi oocytes were defective for embryonic division (fig. 5B).
303 Therefore, in *O. dioica* oogenic meiosis and early embryonic cleavage cycles, Cyclin Ba was
304 required, whereas Cyclin Bc was dispensable.
305 Among the oikopleurids**,** CDK1d and Cyclin Ba specifically appear in *O. dioica* and share several
306 features: X chromosome location, ovary-specific expression, similar degradation dynamics after
307 fertilization (fig. 6B) and similar RNAi phenotypes in meiosis and mitosis. Therefore, we wished to
308 determine if they form an active kinase complex. Cyclin Ba immunoprecipitates possessed H1 kinase
309 activity, whereas lysates from infertile *cycBa* RNAi oocytes lose H1 kinase activity (fig. 5C). This

310 led us to test whether *in intro* constituted odCDK1d-Cyclin Ba complexes possesses kinase activity.
311 GST-odCDK1d recombinants expressed in insect sf9 cells were insoluble. Co-expression with his-
312 Cyclin Ba improved GST-odCDK1d solubility. Purified GST-odCDK1d: his-Cyclin Ba complexes
313 possessed H1 kinase activity (fig. 5E). Surprisingly, the conserved Cyclin B Y170 residue which is
314 critical for CDK1 binding is divergent in odCyclin Ba (replaced by His), whereas it is conserved in
315 odCyclin Bc (supplementary fig. S7). A Y170A substitution is known to completely abolish
316 CDK1:Cyclin B interaction in mouse, human, *Xenopus laevis* and *Ciona intestinalis* (Goda et al.
317 2001; Bentley et al. 2007; Levasseur et al. 2013; Levasseur et al. 2019). The CDK1d:Cyclin Ba
318 complex also has modified residues at the position of the salt bridge (Goda et al. 2001)
319 (supplementary fig. S7), which is in spatial proximity to Y170. This suggests that CDK1d and Cyclin
320 Ba may have coevolved an exclusive interaction that does not interfere with the more canonical
321 CDK1a/b/c:CycBc interactions.

322 **Oscillation of CDK1 levels, instead of Cyclin B levels, orchestrates early embryonic divisions**

323 In marine invertebrates and in *Xenopus* embryos, mitosis is driven by accumulation of Cyclin B to a
324 threshold required to activate CDK1, and mitotic degradation of Cyclin B inactivates CDK1,
325 allowing mitotic exit. Cyclin Ba was stocked in *O. dioica* oocytes and was progressively degraded
326 during early embryogenesis, dropping to low levels by 2.5 hpf (fig. 6A). CDK1d also reached low
327 levels during this same period (fig. 6B). We then performed higher resolution sampling of Cyclin Ba
328 levels at 2 min intervals during the first embryonic cell cycle. Morphologies of the zygotes were
329 recorded at each time point and samples were divided into 2 aliquots and assayed for Cyclin Ba
330 protein levels and H1 kinase activity. Consistent with cell cycle progression, H1 kinase activity
331 oscillated, peaking 20 min post-fertilization, when the nuclear envelope had disappeared and spindles
332 were visible (fig. 6F). H1 kinase levels dropped at 23 min post fertilization, when cleavage furrows
333 formed and dropped to a basal level at 28 min post fertilization, when abscission occurred, and two
334 nuclei were visible. Surprisingly, CDK1d levels oscillated during the first cell cycle (fig. 6 C-G), in
335 contrast to CDK1b and c levels which remained constant. CDK1d levels and H1 kinase activity
336 peaked together at 20 min post fertilization, when NEBD occurred and the spindle assembled.
337 CDK1d levels then peaked again, coincident with a rise in H1 kinase activity during the second cell
338 cycle (fig. 6F and G). To further support this unusual oscillation in CDK1d levels, we labeled oocytes
339 with ^{35}S-methionine, and sampled zygotes after *in vitro* fertilization. Autoradiography of SDS-PAGE
340 detected a 37 KD band at the expected CDK1d MW, which appeared 20 min post-fertilization,
341 corresponding to M phase (fig. 6H). Contrary to the oscillation of CDK1d levels, Cyclin Ba levels
342 did not oscillate during the first 2 embryonic cycles (fig. 6H and G), instead, dropping at later
343 embryonic stages. This latter observation is similar to *Drosophila* preblastoderm cycles, where
344 neither bulk levels of Cyclin B, nor the bulk activity of Cdk1 kinase oscillate, with progressive
345 depletion of maternally stocked Cyclin B only leading to oscillations in Cyclin B levels at later

346 developmental stages (Edgar et al. 1994). A key, and novel difference in *O. dioica* is that CDK1d
347 levels did oscillate during these first embryonic cycles.
348
349 **Discussion**
350 *Oikopleura dioica* exhibits high intrinsic rates of natural population increase (*r*) (0.68 d–1 to 1.07 d–
351 1), well above the normal range for a metazoan of its size (Troedsson et al. 2002). The parameter, *r,*
352 is increased by decreasing generation time, and/or by increasing egg number. In *O. dioica,* generation
353 time is highly heritable and genetically correlated with *r*, whereas fecundity is much less heritable
354 and not genetically correlated with *r* (Lobon et al. 2011). This emphasizes the importance of
355 generation time in setting *O. dioica* fitness and is evidence of a life-history trait that has been strongly
356 constrained by evolution (Deibel and Lowen 2012). The short duration of embryogenesis can be a
357 direct target for selection to increase *r*.
358 We propose a working model for *O. dioica* cell cycle regulation under the framework of multiple
359 CDK1 paralogs during oogenesis and rapid, early embryogenesis (fig. 7). Individual, or combined,
360 knockdowns of CDK1c and e, did not generate any detectable phenotypes. Of note, neither of these
361 CDK1 paralogs was able to complement yeast *cdc28* mutants. Similar to observations in mouse
362 embryos and cultured vertebrate cells, CDK2, the only CDK with a canonical PTSAIRE helix in
363 *Oikopleura,* was dispensable for completion of meiosis and early embryonic divisions, as *CDK2*
364 RNAi zygotes divided and hatched normally (fig. 4A). On the other hand, normal early embryonic
365 divisions required 3 CDK1 paralogs (figs. 4, 5, 7 and supplementary fig. S5), none of which contain
366 a canonical PSTAIRE helix (fig. 1A). Depletion of CDK1a or b alone, delayed embryonic divisions
367 (fig. 3A and B), whereas depletion of CDK1d abolished meiotic NEBD (Ovrebo et al. 2015),
368 disrupted meiosis completion and caused abnormal embryonic cell cycles (fig. 3C-G). Knockdown
369 of CDK1d also depleted oocytes of histone H1kinase activity (Feng and Thompson 2018), as did
370 knockdown of its binding partner, Cyclin Ba (fig. 5C). Double knockdowns of CDK2 and CDK1a
371 arrested zygotes at the pronuclear stage (fig. 4B) whereas double knockdowns of CDK1a and b
372 generated multinucleate embryos with irregular cell division patterns that failed to hatch (fig. 4C and
373 D). CDK1d had critical functions in completion of meiotic M-phases and early embryonic divisions,
374 during which it showed an unusual oscillation of protein levels that peaked in M-phase and decreased
375 during interphase. CDK1d protein dynamics correlated well with the peak of H1 kinase activity and
376 spindle formation during M phase (fig. 6C-H).
377 The 3 CDK1 paralogs are sequentially activated in a tiling pattern when embryos traverse late S-
378 to M-phase, suggesting a further subdivision of CDK1 tasks and substrate targeting, beyond the
379 CDK1-CDK2 subdivision that occurred much earlier in metazoan evolution. An additional,
380 interesting feature of the *O. dioica* CDK1 paralog complement, is that it is CDK1d protein levels
381 rather than its partner, Cyclin Ba, the only essential Cyclin B for *O. dioica* oogenic meiosis and early
382 embryonic cell cycles, which oscillates during early embryonic cell cycles (fig. 6F and G). This

383 contrasts the generally universal oscillation of Cyclin B levels on a background of stable CDK1
384 protein levels characteristic of metazoan cell cycle regulation.
385 During the maternal to zygotic transition, initial, rapid cell cycles, followed by progressive
386 slowing, are a widespread occurrence in a number of species, indicating a consistent benefit to this
387 strategy throughout the evolution of animals with externally deposited eggs (Farrell and O'Farrel
388 2014; Yuan et al. 2016). This strategy converges on modulating the activity of the cell cycle driver,
389 CDK1: weak inhibitory phosphorylation of CDK1 drives rapid cycles without gap phases, and when
390 inhibitory phosphorylation is introduced, catalyzed by Wee and Myt1 kinases, the cell cycle slows
391 and gap phases are inserted (Tsai et al. 2014). *O. dioica* and, the model arthropod, *Drosophila,* are
392 characterized by a number of similarities with respect to oogenesis and early embryogenesis. Both
393 utilize a syncytial strategy during oogenesis (albeit with significant differences in details), where
394 polyploid nurse nuclei generate transcripts that code for materials stocked in the oocytes, which
395 house largely transcriptionally quiescent meiotic nuclei. Both generate excess Cyclin B protein
396 storage in oocytes, with progressive Cyclin B destruction during succeeding embryonic cycles. They
397 diverge, however, in adaptations of rapid mitotic cycles to Cyclin B preloading. *Drosophila* syncytial
398 embryos adapt Cyclin B preloading to mitosis without cytokinesis, compatible with little oscillation
399 of CDK1 kinase levels due to localized Cyclin B destruction (Edgar et al. 1994). In contrast,
400 completion of cytokinesis during the rapid mitoses of *O. dioica* embryonic cycles appears to require
401 oscillation of CDK1 kinase levels (fig. 6F and G). CDK1d oscillations may be an adaptation to the
402 coenocystic ovary structure and Cyclin Ba preloading. Another possible benefit to storage of Cyclin
403 Ba, rather than CDK1d, could be that progressive destruction of Cyclin Ba by the anaphase
404 promoting complex during embryogenesis would deplete Cyclin Ba, facilitating switching of key
405 cell cycle regulators after hatching. In this regard, regulators, such as CDC25, Wee1, and Emi2,
406 critical in controlling important embryonic cell cycle transitions in other organisms (Farrel and
407 O'Farrell 2014; Tsai et al. 2014; Yuan et al. 2016), are all duplicated in the *O. dioica* genome.
408 Coenocystic oogenesis is a common feature of the Oikopleuridae (Ganot et al. 2006), allowing
409 synchronous oocyte growth and maturation as an adaption to a semelparous, opportunistic life style.
410 The oikopleurid lineage also shares the presence of CDK1a, b and c paralogs. This raises questions
411 as to the relationship between the specific gain of the CDK1d-Cyclin Ba complex in *O. dioica*, their
412 linkage on the recently evolved X chromosome, and their ovary-specific expression. This pattern
413 could be explained by resolution of sexual antagonism by gene duplication (Connallon and Clark
414 2011) and higher linkage disequilibrium on the X chromosome (Schaffner 2004). For genes that
415 function both in hermaphrodite ovary and testes, the coenocystic ovary structure evokes conflict
416 between different transcriptional regulation of those genes in polyploid nurse nuclei in the ovary,
417 versus diploid germline progenitor cells in the testis. CDK1c does not show sexually biased gene
418 expression (fig. 2A) (Campsteijin et al. 2012). CDK1c duplication giving rise to CDK1d and e in *O.*
419 *dioica* may have mitigated sexual antagonistic conflict by allowing CDK1d (sexually biased

420 expression to ovaries) to evolve essential ovarian functions. The X chromosome location of CDK1d
421 might facilitate CDK1d ovary-specific expression since duplicates beneficial to females
422 preferentially accumulate on the X chromosome where they are exposed to selection twice as often
423 in females versus males (Connallon and Clark 2011). Indeed, when compared to zygotic promoters,
424 maternal promoters in *O. dioica* are located on the X-chromosome more frequently than expected,
425 ($\chi 2 = 43.34$, df = 1, $p = 4.61 \times 10^{-11}$), revealing a female-bias of X-linked genes in *O. dioica* (Danks
426 et al. 2018). X-linkage of *CDK1d* and *Cyclin Ba* loci would then efficiently sustain linkage
427 disequilibrium, reinforced through selection on the recently formed X chromosome (Bachtrog et al.
428 2009). Since there will be no recombination in the heterogametic male, this would contribute to an
429 increase in sweeping to fixation in the population.

430 In *O. dioica*, the 3 CDK1 paralogs (a, b and d), which are required for correction execution of early
431 embryonic cell cycles, exhibit sequence diversification on their activation segments, ATP binding
432 sites and Cyclin B interaction interfaces. This raises the possibility of different k_{cat}/k_m catalytic
433 outputs or phosphorylation site specificities during these rapid cell cycles. With respect to the K89
434 residue in the hinge region, both CDK1a and b, which participate in events preceding CDK1d, share
435 a K89E/D substitution. This substitution would likely reduce CDK1 k_{cat}. CDK1a, b and d also have
436 non-overlapping activation segments, suggesting CDK1 paralogs may have different affinities
437 toward the same substrate phosphorylation site and/or different phosphorylation site preferences. The
438 sequential activation of CDK1a, b and d may provide a more stepwise, as opposed to progressive,
439 increase of kinase activity, which may enhance and sharpen transitions towards early, middle and
440 late substrates across early embryonic cell cycles. In metazoan cell cycles, the division of labor
441 between CDK1 and CDK2 is not absolute. CDK1 retains essential roles in late S phase that CDK2
442 does not efficiently complement (Katsuno et al. 2009; Nakanishi et al. 2010; Farrell et al. 2012).
443 Inactivation of Cdk1 in temperature-sensitive Cdk1 mutant cell lines (FT210) resulted in a prolonged
444 S phase accompanied by ineffective firing of late replicon clusters and reduced the density of active
445 origins during late S phase (Katsuno et al. 2009). In *Drosophila* pre-mild blastula transition S phases,
446 it is Cdk1 activity, rather than Cdk2 activity that regulates late replication (Farrell et al. 2012; Seller
447 and O'Farrell 2018). The requirement for CDK1 in late S phase, coexists with its need to be repressed
448 during early S phase (Larochelle et al, 2007) and its control in late S phase by Chk1 (Lemmens et al.
449 2018), to prevent premature triggering of M phase (Szmyd et al. 2019). In *O. dioica*, the conflict of
450 CDK1's roles in the metazoan cell cycle of regulating both late S and M phase, might be relaxed by
451 CDK1 duplication and subsequent partitioning of ancestral CDK1's roles in S and M phase to
452 specific paralogs. Our results indicate that CDK1a collaborates with CDK2 to drive S phase and
453 suggest that this paralog may exhibit reduced risk of triggering M phase, through lower intrinsic
454 kinase activity, arising from substitution in hinge region (supplementary fig. S2). On the other hand,
455 the CDK1d paralog has become a specialist of M phase events without additional constraints imposed

456 by regulation of late DNA replication. This may reflect adaptation to very rapid embryonic cell
457 divisions in this planktonic organism.
458 A conformation change of the very highly conserved PSTAIRE helix is central to CDK1
459 inactivation/activation transitions (Huang et al. 2012). It is therefore surprising that this sequence
460 was modified in all *O. dioica* CDK1 paralogs. *O. dioica* CDK2, the only CDK in this species with a
461 conserved PSTAIRE, was dispensable for embryonic divisions, recalling the situation in plants,
462 where the CDK1 ortholog, CDKA, which has the canonical PSTAIRE, is dispensable for the cell
463 cycle, whereas CDKB, deviating in the PSTAIRE, has essential functions in the absence of CDKA
464 (Nowack et al. 2012). Strikingly, the modified PSTAIRE of the *O. dioica* CDK1d paralog
465 (PPTSLRE) shows convergence over great evolutionary distance with plant CDKB sequences
466 (P[P/S]T[A/T]LRE), and in both *O. dioica*, and plants, these variants exhibit increased specialization
467 to M-phase (Joubes et al. 2000; Nowack et al. 2012). The suite of naturally evolved *O. dioica*,
468 CDK1:Cyclin B complexes, with critical residue substitutions in their activation segments, ATP
469 binding sites, CDK1-Cyclin B interaction interfaces, and Cyclin B-substrate interaction elements,
470 provide a fertile foundation for structural studies of how these changes elicit enhanced kinase
471 selection for subsets of G2-M, CDK1 cell cycle substrates.
472

473 **Materials and Methods**

474 **Animal culture and collection**

475 *O. dioica* were maintained in culture at 15°C (Bouquet et al. 2009). Day 4–6 animals were placed in
476 filtered seawater, removed from their houses and anesthetized in cold ethyl 3-aminobenzoate
477 methanesulfonate salt (MS-222, 0.125 mg/ml; Sigma) before collection.

478 ***In vitro* fertilization (IVF) and collection of synchronously dividing zygotes**

479 Sperm solutions were prepared by transferring 5 mature males to a petri dish containing 10 ml
480 artificial seawater, on ice, and sperm quality was assessed using a Nikon Eclipse E400 microscope.
481 Mature females were transferred to artificial sea water in 24-well plates coated with 0.9% agarose,
482 artificial sea water was changed every hour. Oocytes were fertilized with 400 µl sperm solution and
483 fertilized oocytes were washed in 8 ml artificial sea water within 50 seconds. Synchronicity of
484 fertilization was verified by following polar body exclusion and early cleavages.

485 **Phylogenetic Analyses**

486 A search of larvacean CDK1, CDK2 and Cyclin B proteins was performed using TBLASTN against
487 genomes and transcriptomes of *Oikopleura albicans, O. longicauda, O. vanhoeffeni and Fritillaria*
488 *borealis*. *O. dioica* CDK1, CDK2 and Cyclin Bc were used as queries with E-value cutoff set to 1e-
489 005. *Ciona intestinalis* and *Branchiostoma floridae* proteins were obtained from the JGI Genome
490 Portal (https://genome.jgi.doe.gov/mycocosm/home). For identified targets, amino acid sequences of
491 the N-terminal cyclin box or the kinase domain of CDK1/2 were aligned (clustalX). Alignments were

492 manually edited (Bio-edit), and secondary structure analysis (psipred) was used to guide alignments.
493 Phylogenetic relationships were inferred using maximum likelihood (ML) using MEGA7 (Kumar et
494 al. 2016), with amino acid sequence alignment based on Jones-Taylor-Thornton (Jones et al 1992).
495 Estimates of the gamma-shape parameter and proportion of invariant sites were then used to obtain
496 the 500 bootstrap replicates.

497 **Yeast Complementation**

498 We used a W303a-background yeast wild-type strain SCU893 (*MATa ura3 ade2-1 trp1-1 leu2-3112*
499 *his3-11 bar1::hisG*) and its derivative SCU112 (*cdc28-4*). To complement a *cdc28* mutation of *S.*
500 *cerevisiae*, the open reading frames of the *O. dioica CDK1* paralogs and *CDK2* cDNAs were cloned
501 in pCR™4-TOPO® TA Vector (Thermofisher). cDNA fragments were isolated by digestion with
502 *EcoR*I and *Not*I and ligated into the yeast pYES2 expression vector (Invitrogen) downstream of the
503 inducible GAL1 promoter. The resulting CDK1 paralog plasmids were individually transformed by
504 the lithium acetate method (Ito et al. 1984) into the *S. cerevisiae cdc28-4* strain. As a control, *cdc28-*
505 *4* was transformed with the empty pYES2 vector. The transformants were grown for 4 days at 25°C,
506 and the resulting colonies were cultivated overnight at 25°C in CM-ura medium containing glucose
507 as a carbon source. The cells were pelleted, washed, resuspended in CM-ura medium containing 2%
508 glycerol, and grown further at 25°C. After 4 h, the cells were pelleted and resuspended in CM-ura
509 medium containing either glucose (2%), or galactose (2%)–raffinose (1%) as carbon source, and
510 grown at 25°C, or the restrictive 36°C, respectively.

511 **Antibodies**

512 Rabbit polyclonal affinity–purified anti-Cyclin Ba/b (acetyl-NRDLNIQESGPVKAVVNAC-amide;
513 acetyl-CLEFLRRFSRVAEETIDPKEY-amide), anti-CDK1b (acety1-
514 CPDFTKPSTLNVNTSLNEMDM-amide), anti-CDK1c (acetyl-MRKRNIDRPPTQDLNNYC–
515 amide), ant-Cdk1d (acety1-MIKAKSGTQDLSNYKRC-amide), and anti-lamin1 (acetyl-
516 QSPISLPPLSGSTC-amide) were from 21st Century Biochemicals (Marlboro, MA). Other
517 antibodies: anti-PSTAIR (Abcam, ab10345), anti-ATPB (Abcam, ab37922), anti-histone 3 (Abcam,
518 ab10799). Secondary antibodies for immunofluorescence: goat anti-rabbit IgG (H+L) Alexa Fluor
519 568 (Thermofisher, A-11011); and for western blots: goat anti-rabbit IgG (H+L) superclonal™
520 secondary antibody, HRP (Thermofisher, A27033), Peroxidase-AffiniPure Goat Anti-Mouse IgG
521 (H+L) (Jackson ImmunoResearch, 115-035-003).

522 **Quantitative Reverse Transcription–PCR, Immunofluorescence and Western Blots**

523 Total RNA was isolated from snap-frozen animals. For qRT-PCR, 1 µg of purified total RNA was
524 subjected to RT using M-MLV reverse transcriptase (Invitrogen). The quantitative polymerase chain
525 reaction (qPCR) (CFX-96; Bio-Rad) was performed using cDNA templates synthesized from an
526 equivalent of 5 ng total RNA, 10 µl of qPCR 2 Master Mix (Bio Rad), and 500 nM primers in a total

527 volume of 20 µl. After initial denaturation for 5 min at 95 °C, 45 cycles of 95 °C for 15 s, 60 °C for
528 20 s, and 72 °C for 20 s were conducted, with a final extension for 5 min at 72 °C. RT-negative
529 controls were run to 45 cycles. RPL23 and EF-1β mRNA levels served as normalization controls in
530 all qRT-PCRs. For RNAi experiments, target mRNA levels were normalized to control zygotes.
531 Primer pair specificities were confirmed by melting curve evaluation, cloning, and sequencing of
532 amplicons. In these experiments, mean values normalized to EF-1β control transcripts are presented.
533 Immunofluorescence and Western blots were performed as previously (Campsteijn et al. 2012).

534 **Microinjection**

535 Gonad microinjections were performed as previously (Ovrebo et al. 2015). Injection solutions were
536 prepared by mixing 300 ng/µl double stranded RNA (dsRNA) in RNase free PBS. Anesthetized day
537 4 animals in filtered seawater were transferred to Petri dishes coated with 2% agarose. Gonads were
538 injected on a Nikon Eclipse TE2000-S inverted microscope equipped with Narishige
539 micromanipulators and transjector 5246 micro injector (Eppendorf). Injected day 4/5 animals were
540 transferred to watch glasses containing filtered seawater for recovery and then transferred to 6 L
541 beakers for subsequent culture. Animals were cultured until spawning for in vitro fertilization (IVF)
542 and immunofluorescence. Before oocyte injection, oocytes were transferred to 24-well plate coated
543 with 0.9% agarose containing fresh artificial seawater (Red Sea) for 1 h. Samples of 50 oocytes were
544 used for qRT-PCR. Remaining oocytes were fertilized and developmental defects arising from
545 various treatments were assessed by unpaired Student's t-test for equal variances, or, unpaired,
546 Welch's t-test for unequal variances. Effect size was calculated as Cohen's $d = 2t/\mathrm{SQRT}\ (df)$.

547 ***In vitro* CDK1 kinase activities**

548 CDK1 kinase activities were determined as previously (Feng and Thompson 2018). Equal numbers
549 of oocytes were snap frozen and thawed twice. Cyclin Ba immunoprecipitates, purified his-Cyclin
550 Ba-GST OdCdk1d complexes were aliquoted, kept at 80°C and thawed before use. Samples were
551 mixed with biotinylated MV peptide and 1 mM ATP incubated at 30°C for 30 min. After stopping
552 the phosphorylation reaction, ELISA was performed using anti-phospho MV peptide antibody
553 (MESACUP) and the CDK1 Kinase Assay Kit (MBL). Finally, POD-conjugated streptavidin was
554 used to detect phosphorylated MV peptide and color development measured at 492 nm. Differences
555 in CDK1 kinase activities from different knockdown treatments were assessed by the Student's T-
556 test. H1 kinase assays were performed as previously (Levasseur and McDougall 2000). After thawing
557 snap frozen oocyte samples on ice, 2 µl of 6× kinase reaction mixture (pH 7.2) containing histone
558 H1 (Sigma type III from calf thymus), 0.6 mM ATP, 0.5 mCi/ml $^{[32P]}$ATP, and 60 µM cAMP-
559 dependent protein kinase inhibitor was added to 10 µl of oocyte sample. The reaction was started by
560 transfer to a 30°C heat block for 30 min and stopped by adding 5× Laemmli buffer. The samples
561 were then heated to 80°C for 10 minutes and resolved on 15% polyacrylamide gels. Gels were placed
562 in a Phosphorimager (Fujix; 1500 Bas Reader) and incorporation of [^{32}P] was quantified.

563 **Metabolic labeling of zygotes**

564 Unfertilized oocytes obtained from individual females were transferred into one well of 24-well plate
565 coated with 0.9% agarose. After addition of a mixture of ^{35}S-labeled amino acids (Pro-mix,
566 Amersham) to a final concentration of 330 µCi/ml and incubation for 60 min at room temperature,
567 oocytes were fertilized and harvested at different times post fertilization. The samples were briefly
568 centrifuged to eliminate excess of labeled mixture and 5x Laemmli buffer was added to the pellets.
569 Samples were then heated to 80°C for 10 min and resolved on 10% polyacrylamide gels. Gels were
570 stained with 0.5% Coomassie blue R250 in 45% methanol, 45% water, 10% acetic acid, and
571 destained in 20% methanol, 75% water, 5% acetic acid; and dried on Whatman 3MM paper. Dried
572 gels were autoradiographed using a Phosphorimager (Fujix; 1500 Bas Reader).

573 **Capped mRNA and dsRNA synthesis**

574 For indestructible Cyclin Ba injection, site directed mutagenesis (New England Biolabs) was used to
575 delete the destruction box (NTEREQLQALN) using a cyclin Ba/b entry clone as template with
576 subsequent recombination with pSPE3-Venus-RfA. The resulting plasmid was used as a template for
577 PCR amplification. Amplicons were purified by phenol-chloroform extraction followed by ethanol
578 precipitation. Capped mRNAs were synthesized from these templates using mMessage mMachine
579 (Ambion) followed by poly(A) tailing (Ambion) according to the manufacturer's protocol and
580 purified by Lithium chloride precipitation. DNA templates for dsRNA synthesis were prepared by
581 PCR using gene-specific primers with T7 overhang and purified by phenol-chloroform extraction.
582 Sense and antisense RNA were synthesized in a single reaction following the recommended protocol
583 using T7 RiboMAX™ Express RNAi system (Promega).

584

585 **Acknowledgments and funding information**

586 We thank Haiyang Feng, for helpful discussion and A. Aasjord and K. N. Nøkling for providing
587 animals from the *Oikopleura* culture facility. Yeast strains were provided by Jorrit Enserink, Univ.
588 of Oslo. We thank the Chourrout S1 group at the Sars Centre for early access to sequence data from
589 hermaphroditic appendicularian species. *Oikopleura dioica* genome and transcriptome are available
590 at http://www.genoscope.cns.fr http://oikoarrays.biology.uiowa.edu/Oiko/ and transcription start site
591 CAGE data at the NCBI Gene Expression Omnibus https://www.ncbi.nlm.nih.gov/geo/ under
592 accession number GSE78794. The *Fritillaria borealis* genome is available at GenBank
593 https://www.ncbi.nlm.nih.gov/genbank/: SDII00000000 and other *Oikopleura* species genomes at
594 GenBank SCLD01000000 to SCLH01000000. This work was supported by grants 183690/S10 NFR-
595 FUGE and 133335/V40 from the Norwegian Research Council (E.M.T.).

596 **Author Contributions**

X.M., and E.M.T. conceived and designed the experiments. X.M. performed experiments and X.M. and E.M.T. analyzed the data. J.I.Ø performed CDK1-GFP cmRNA injection and immunostaining. X.M. and E.M.T. wrote the manuscript. All authors approved the manuscript.

Figure Legends

FIG. 1 Amplification of CDK1 paralogs in the *Oikopleura* genus. (*A*) Left panel: Maximum likelihood inference analysis of selected chordate CDK1 proteins using the kinase domain of CDK1s with bootstrap values indicated at nodes. bn/bs values in all branches were calculated using a modified Nei-Gojobori method (Zhang et al. 1998). Blue branches have significant bn/bs values over 1 as determined by one-sided Z tests: lineage subtending CDK1a, P = 0.0386; lineage subtending CDK1b, P = 0.0305, lineage subtending CDK1c, P = 0.0334. Modifications in the highly conserved PSTAIRE domain of each CDK1 are shown. The codons resulting in the alanine to serine substitution within the Oikopleuridae (dark grey box) are also indicated. Codons for serine with phase 2 intron insertions (splitting codons between the second and third nucleotides) are denoted by "2". (*B*) Maximum likelihood inference analysis of selected chordate Cyclin B proteins. The Oikopleuridae paralogs are indicated by a grey box. (*C*) CDK1 paralog localizations on chromosomes among appendicularians. Arrows indicate possible chronological duplication steps and chromosomal translocations consistent with the phylogenetic analyses. (*D*) Complementation studies using budding yeast cdc28-4ts mutants substituted with *O. dioica* CDK1 paralogs. CDK1a, b and d paralogs were able to complement whereas c and e did not. (*E*) Alternative *CDK1d* transcription start sites (TSS) in testes versus ovaries. CDK1d maternal transcripts have a broad TSS before the ATG start codon. Testes *CDK1d* transcripts originated from a single TSS immediately before the AG splice acceptor site of fist intron, 42 nt downstream of the TCTAGA male-specific promoter element, which is also located within the first intron. Male *CDK1d* transcripts lack an ATG start codon, and yield nonsense transcripts in all three possible reading frames. Vertical axis scale for CAGE data (Danks et al. 2018) is in reads per million.

FIG. 2. CDK1 and Cyclin B paralog expression profiles. (*A*) *CDK1-Cyclin B* paralog expression levels during gonad maturation from Day 3 to spawning. Expression data were normalized to transcription of the EF1b and Rpl23 housekeeping genes. Levels are normalized to maximum levels. (*B*) Western blots of CDK1-Cyclin B paralog levels during development, gonad maturation and embryogenesis.

FIG. 3. *CDK1a*, *b*, and *d* knockdowns generate abnormal embryonic phenotypes. (*A*) *CDK1a* RNAi delays embryonic divisions and tadpoles fail to form. Left panel: efficient knockdown of *CDK1a* in oocytes spawned from ovaries injected with dsRNA against *odCDK1a* at D5. Mid panel: When exposed to wild-type sperm, *CDK1a* deficient oocytes generated embryos that divided more slowly than wild-type and failed to hatch at 4 hpf. Right panel: images of delayed development in

632 CDK1a deficient embryos. When wild-type embryos had developed to the late tailbud stage, CDK1a
633 deficient embryos had only begun to gastrulate. At 7 hpf, tadpoles were observed in wild-type
634 whereas CDK1a deficient embryos failed to reach the tailbud stage. The legend in (*A*) also applies to
635 the respective panel in (*B*). (*B*) Upper left panel: efficient knockdown *CDK1b* in oocytes spawned
636 from ovaries injected with dsRNA against *odCDK1b* at D5. Upper mid panel: When exposed to wild-
637 type sperm, *CDK1b* deficient oocytes generated embryos that failed to hatch at 4 hpf. Upper right
638 panel: Western blot showing absence of CDK1b protein in *CDK1b* RNAi embryos. Bottom left
639 panel: CDK1b deficient embryos arrested before gastrulation. Lower right panel: distribution of
640 developmental stages in *CDK1b* deficient and wild type embryos assessed at 1 hpf. (*C-E*),
641 Knockdown of *CDK1d* generated 3 different phenotypes at 1 hpf. Left panels reveal efficient
642 knockdown in oocytes spawned from ovaries that had been injected with dsRNA against *odCDK1d*
643 at D5. Right panels revealed abnormal division in all cases with a subset of embryos exhibiting more
644 severe phenotypes of polar body extrusion but no cell division, or a complete lack of polar body
645 extrusion and absence of any division. The legend in (*E*) also applies to the respective panels in (*C*)
646 and (*D*). (*F*) Knockdown of CDK1d did not have any effect on the levels of Cyclin Ba, the Cyclin
647 component of MPF in *O. dioica* oocytes (Feng and Thompson 2018). (*G*) Image comparisons of wild-
648 type to *CDK1d* knockdown oocyte/embryo phenotypes 1 h post exposure to wide type sperm. Left
649 to right: WT cleavage stage embryos, infertile oocytes with no polar body extrusion, polar bodies
650 extruded, but no division, and abnormally dividing embryos. Where indicated, ***P<0.001,
651 **P<0.01, *P<0.05. Scale bars: 50 µm.

652 **FIG. 4. CDK2 is dispensable for *Oikoplerua dioica* embryogenesis. Synergistic defects of *CDK2*
653 **+ *CDK1a* RNAi and *CDK2* + *CDK1b* RNAi in embryonic divisions.** (*A*) CDK2 is dispensable for
654 embryonic divisions. Right panel: efficient knockdown of *CDK2* in oocytes and tadpoles, spawned
655 from ovaries injected with dsRNA against *odCDK2* at D4. Mid panel: Western blot showing absence
656 of CDK2 protein in *CDK2* RNAi oocytes and tadpoles. Right panel: no significant differences in
657 developmental outcome between *CDK2* deficient and wild-type embryos. (*B*) Synergistic effect of
658 *CDK2* + *CDK1a* RNAi on embryonic divisions. Left Panel: efficient knockdown of *CDK1a* and
659 *CDK2* in oocytes from ovaries that had been injected with dsRNA against *odCDK2* and *CDK1a* at
660 D5. Mid panel: Western blot showing absence of CDK2 protein in CDK1a + *CDK2* RNAi in oocytes.
661 Right panel: at 45 min pf, *CDK1a* + *CDK2* deficient zygotes were arrested prior to pronuclear fusion.
662 Scale bars: 50 µm. (*C*) Synergistic effect of *CDK1a* + *b* RNAi on embryonic division. Upper left
663 panel: efficient knockdown of *CDK1a* and in oocytes from ovaries that had been injected with
664 dsRNA against *CDK1a* + *b* at D5. Lower left: Western blot showing absence of CDK1b protein in
665 *CDK1a* + *b* RNAi oocytes. Right panel: *CDK1a* + *b* deficient zygotes finished 3 rounds of slowed
666 divisions before arresting at the 4th-5th embryonic division. Scale bars: 50 µm. Where indicated,
667 ***P<0.001, **P<0.01, *P<0.05. (*D*) Confocal images of Lamin 1 and DNA staining of wild-type

668 versus *CDK1a* + *b* RNAi embryos at 80 min post-fertilization. *CDK1a* + *b* deficient zygotes arrest
669 at prophase with super-condensed chromosomes at the nuclear periphery (inset) after the third
670 division. Scale bars: 20 µm.

671 **FIG. 5. Cyclin Ba, is required for *O. dioica* embryonic cell cycles, whereas Cyclin Bc is**
672 **dispensable.** (*A*) Cyclin Bc is dispensable for embryonic divisions. Left panel: efficient knockdown
673 *cycBc* in oocytes and tadpoles spawned from ovaries that had been injected with dsRNA against
674 *cycBc* at D5. Mid panel: no significant difference in mean H1 kinase activity between Cyclin Bc
675 deficient and wild-type oocytes (metaphase I arrested). Upper right panel: Western blot showing that
676 knockdown of *cycBc* had no effect on protein levels of Cyclin Ba. Lower right panel: images show
677 Cyclin Bc deficient and wild-type embryos had identical phenotypes at the tailbud stage, 4 hpf. (*B*)
678 Efficient knockdown of *cycBa* in oocytes spawned from ovaries that had been injected with dsRNA
679 against *cycBa* at D5. Cyclin Ba deficient oocytes exposed to wild-type sperm generated two
680 embryonic phenotypes: infertile and abnormal divisions. Abnormal division phenotypes, compared
681 to wild-type, are illustrated in the bottom panels at 1 hpf. Where indicated, ***P<0.001, **P<0.01,
682 *P< 0.05. (*C-E*) CycBa-CDK1d complexes have histone H1 kinase activity. (*C*) H1 kinase activity
683 assay was present in wild type oocytes but absent in *cycBa* RNAi knockdown oocytes (Feng and
684 Thompson 20118). (*D*) Cyclin Ba immunoprecipitates from oocytes had H1 kinase activity whereas
685 IgG oocyte immunoprecipitates did not. (*E*) H1 kinase activity levels of *O. dioica* Cyclin Ba
686 pulldowns compared to IgG pulldowns and *in vitro* expressed complexes of Human (Hs)
687 CDK1:Cyclin B1 and *O. dioica* (Od) CDK1d:Cyclin Ba. Scale bars: 50 µm.

688 **FIG. 6. CDK1d levels oscillate during early embryonic cell cycles.** (*A*) Cyclin Ba levels do not
689 oscillate but instead, decline steadily during early embryogenesis. Upper panel: Western blot of
690 Cyclin Ba during the first 4 h of development with ATPase beta as a loading control. Lower panel:
691 quantification of Cyclin Ba levels, normalized to levels in unfertilized oocytes. (*B*) Upper panel:
692 Western blot of CDK1d levels during the first 4 h of development with histone H3 as a loading
693 control. Lower panel: *CDK1d* mRNA levels were quantified during early embryonic development
694 by qRT-PCR, normalized to levels in unfertilized oocytes. (*C-E*) CDK1d levels peaked in M phase
695 of first two mitotic embryonic cell cycles. (*C*) Western blot of CDK1b, c, and d levels during the first
696 3 hpf. Arrow indicates the CDK1d band. I, interphase; M, M-phase. (*D*) Sampling of CDK1d levels
697 at 1-minute internals around M phase of the first embryonic cell cycle. Arrow indicates the oscillation
698 of the CDK1d band. (*E*) Sampling of CDK1d levels around M-phase of the second division cycle.
699 Arrow indicates the oscillation of the CDK1d band. (*F*) Western blot analyses of Cyclin Ba levels
700 and histone H1 kinase activity during the first two embryonic cell cycles. Cyclin Ba levels remained
701 elevated, whereas H1 kinase activity oscillated, with peaks in the first two M-phases. (*G*)
702 Quantification of Cyclin Ba, CDK1d and H1 kinase activity during the first two embryonic cell
703 cycles. (*H*) Oocytes were incubated in artificial sea water with 35S methionine for 1 h before

704 fertilization. Embryos were collected at 3 min intervals during the course of first embryonic cell
705 cycle. The autoradiograph shows *de novo* synthesized protein during the course of this cycle. Arrow
706 indicates the CDK1d band.

707 **F$_{IG}$. 7. Sequential activation of CDK1a, b and d, and switching from oscillations of CDK1d**
708 **levels to oscillation of Cyclin Ba levels, drive rapid early embryonic cell cycles in *O. dioica*.**
709 Knockdowns revealed that sequential activation of 3 *O. dioica* CDK1 paralogs, a, b and d, are
710 required for proper execution of embryonic divisions leading to embryo hatching. Cyclin Ba, the
711 partner of CDK1d, is maternally stocked and gradually degrades over the first embryonic cycles,
712 whereas unusually, it is CDK1d protein levels that initially oscillate to regulate rapid M-phases.
713 CDK1a and b levels remain constant during this period. During the maternal to zygotic transition,
714 the cell cycle slows and divisions become less synchronous. In the coenocystic ovary, polyploid
715 nurse nuclei are afforded the time to produce maternally stocked transcripts, many arising from genes
716 containing multiple introns of variable length, with the genes often organized in polycistronic
717 operons (Danks et al. 2015). During the period of rapid embryonic cell divisions, many zygotically
718 activated genes are monocistronic, and contain short introns, or are intronless.
719

720 **References**

721 Ahn SH, Tobe BT, Gerald JNF, Anderson SL, Acurio A, Kron SJ. 2001. Enhanced cell polarity in
722 mutants of the budding yeast cyclin-dependent kinase Cdc28p. *Mol Biol Cell* 12(11):3589-3600.
723 Arooz T, Yam CH, Siu WY, Lau A, Li KKW, Poon RYC. 2000. On the concentrations of cyclins
724 and cyclin-dependent kinases in extracts of cultured human cells. *Biochemistry* 39(31):9494-
725 9501.
726 Bachtrog D, Jensen JD, Zhang Z. 2009. Accelerated adaptive evolution on a newly formed X
727 chromosome. *Plos Biol.* 7(4):e1000082
728 Bao ZQ, Jacobsen DM, Young MA. 2011. Briefly bound to activate: Transient binding of a second
729 catalytic magnesium activates the structure and dynamics of cdk2 kinase for catalysis. *Structure*
730 19(5):675-690.
731 Bentley AM, Normand G, Hoyt J, King RW. 2007. Distinct sequence elements of cyclin B1
732 promote localization to chromatin, centrosomes, and kinetochores during mitosis. *Mol Biol Cell*
733 18(12):4847-4858.
734 Bouquet JM, Spriet E, Troedsson C, Ottera H, Chourrout D, Thompson EM. 2009. Culture
735 optimization for the emergent zooplanktonic model organism *Oikopleura dioica*. *J Plankton*
736 *Res*. 31(4):359-370.
737 Brown NR, Korolchuk S, Martin MP, Stanley WA, Moukhametzianov R, Noble MEM, Endicott
738 JA. 2015. Cdk1 structures reveal conserved and unique features of the essential cell cycle Cdk.
739 *Nat Commun*. 6:e6769
740 Brown NR, Noble MEM, Endicott JA, Johnson LN. 1999. The structural basis for specificity of
741 substrate and recruitment peptides for cyclin-dependent kinases. *Nat Cell Biol.* 1(7):438-443.
742 Campsteijn C, Ovrebo JI, Karlsen BO, Thompson EM. 2012. Expansion of cyclin D and Cdk1
743 paralogs in *Oikopleura dioica*, a chordate employing diverse cell cycle variants. *Mol Biol Evol*.
744 29(2):487-502.

745 Chen C, Ha BH, Thevenin AF, Lou HJ, Zhang R, Yip KY, Peterson JR, Gerstein M, Kim PM,
746 Filippakopoulos P et al. 2014. Identification of a major determinant for serine-threonine kinase
747 phosphoacceptor specificity. *Mol Cell* 53(1):140-147.
748 Connallon T, Clark AG. 2011. The resolution of sexual antagonism by gene duplication. *Genetics*
749 187(3):919-937.
750 Creixell P, Palmeri A, Miller CJ, Lou HJ, Santini CC, Nielsen M, Turk BE, Linding R. 2015.
751 Unmasking determinants of specificity in the human kinome. *Cell* 163(1):187-201.
752 Danks GB, Navratilova P, Lenhard B, Thompson EM. 2018. Distinct core promoter codes drive
753 transcription initiation at key developmental transitions in a marine chordate. *BMC Genomics*
754 19:164
755 Danks GB, Raasholm M, Campsteijn C, Long AM, Manak JR, Lenhard B, Thompson EM. 2015.
756 Trans-splicing and operons in metazoans: Translational control in maternally regulated
757 development and recovery from growth arrest. *Mol Biol Evol.* 32(3):585-599.
758 Deibel D, Lowen B. 2012. A review of the life cycles and life-history adaptations of pelagic
759 tunicates to environmental conditions. *ICES J Mar Sci. 69*(3):358-369.
760 Des Marais DL, Rausher MD. 2008. Escape from adaptive conflict after duplication in an
761 anthocyanin pathway gene. *Nature* 454(7205):762-785.
762 Echalier A, Cot E, Camasses A, Hodimont E, Hoh F, Jay P, Sheinerman F, Krasinska L, Fisher D.
763 2012. An integrated chemical biology approach provides insight into Cdk2 functional
764 redundancy and inhibitor sensitivity. *Chem Biol.* 19(8):1028-1040.
765 Edgar BA, Orr-Weaver TL. 2001. Endoreplication cell cycles: More for less. *Cell* 105(3):297-306.
766 Edgar BA, Sprenger F, Duronio RJ, Leopold P, O'Farrell PH. 1994. Distinct molecular
767 mechanisms regulate cell-cycle timing at successive stages of *Drosophila* embryogenesis. *Gene*
768 *Dev.* 8(4):440-452.
769 Farrell JA, O'Farrell PH. 2014. From egg to gastrula: How the cell cycle is remodeled during the
770 *Drosophila* mid-blastula transition. *Annu Rev Genet.* 48:269-294.
771 Farrell JA, Shermoen AW, Yuan K, O'Farrell PH. 2012. Embryonic onset of late replication
772 requires Cdc25 down-regulation. *Gene Dev*. 26(7):714-725.
773 Feng HY, Thompson EM. 2018. Specialization of Cdk1 and cyclin B paralog functions in a
774 coenocystic mode of oogenic meiosis. *Cell Cycle* 17(12):1425-1444.
775 Fleig UN, Gould KL, Nurse P. 1992. A dominant negative allele of p34(cdc2) shows altered
776 phosphoamino acid content and sequesters p56(cdc13) cyclin. *Mol Cell Biol.* 12(5):2295-2301.
777 Ganot P, Bouquet JM, Kallesoe T, Thompson EM. 2007. The *Oikopleura* coenocyst, a unique
778 chordate germ cell permitting rapid, extensive modulation of oocyte production. *Dev Biol.*
779 302(2):591-600.
780 Ganot P, Bouquet JM, Thompson EM. 2006. Comparative organization of follicle, accessory cells
781 and spawning anlagen in dynamic semelparous clutch manipulators, the urochordate
782 Oikopleuridae. *Biol Cell* 98(7):389-401.
783 Ganot P, Thompson EM. 2002. Patterning through differential endoreduplication in epithelial
784 organogenesis of the chordate, *Oikopleura dioica*. *Dev Biol.* 252(1):59-71.
785 Goda T, Funakoshi M, Suhara H, Nishimoto T, Kobayashi H. 2001. The N-terminal helix of
786 *Xenopus* cyclins A and B contributes to binding specificity of the cyclin-Cdk complex. *J Biol*
787 *Chem.* 276(18):15415-15422.
788 Holt LJ, Tuch BB, Villen J, Johnson AD, Gygi SP, Morgan DO. 2009. Global analysis of Cdk1
789 substrate phosphorylation sites provides insights into evolution. *Science 325*(5948):1682-1686.
790 Huang H, Zhao RJ, Dickson BM, Skeel RD, Post CB. 2012. Alpha C helix as a switch in the
791 conformational transition of Src/Cdk-like kinase domains. *J Phys Chem B* 116(15):4465-4475.

792 Ito H, Murata K, Kimura A. 1984. Transformation of intact yeast-cells treated with alkali cations or
793 thiol compounds. *Agr Biol Chem.* 48(2):341-347.
794 Jeffrey PD, Ruso AA, Polyak K, Gibbs E, Hurwitz J, Massague J, Pavletich NP. 1995. Mechanism
795 of Cdk activation revealed by the structure of a cyclina-Cdk2 complex. *Nature*. 376(6538):313-
796 320.
797 Jones DT, Taylor WR, Thornton JM. 1992. The rapid generation of mutation data matrices from
798 protein sequences. *Comput Appl Biosci.* 8(3):275-282.
799 Joubes J, Chevalier C, Dudits D, Heberle-Bors E, Inze D, Umeda M, Renaudin JP. 2000. Cdk-
800 related protein kinases in plants. *Plant Mol Biol.* 43(5-6):607-620.
801 Katsuno Y, Suzuki A, Sugimura K, Okumura K, Zineldeen DH, Shimada M, Niida H, Mizuno T,
802 Hanaoka F, Nakanishi M. 2009. Cyclin A-Cdk1 regulates the origin firing program in
803 mammalian cells. *Proc Natl Acad Sci USA.* 106(9):3184-3189.
804 Koivomagi M, Valk E, Venta R, Iofik A, Lepiku M, Morgan DO, Loog M. 2011. Dynamics of
805 Cdk1 substrate specificity during the cell cycle. *Mol Cell* 42(5):610-623.
806 Kumar S, Stecher G, Tamura K. 2016. MEGA7: Molecular evolutionary genetics analysis version
807 7.0 for bigger datasets. *Mol Biol Evol.* 33(7):1870-1874.
808 Larochelle S, Merrick KA, Terret ME, Wohlbold L, Barboza NM, Zhang C, Shokat KM, Jallepalli
809 PV, Fisher RP. 2007. Requirements for Cdk7 in the assembly of Cdk1/cyclin B and activation
810 of Cdk2 revealed by chemical genetics in human cells. *Mol Cell* 25(6):839-850.
811 Lemmens B, Hegarat N, Akopyan K, Sala-Gaston J, Bartek J, Hochegger H, Lindqvist A. 2018.
812 DNA replication determines timing of mitosis by restricting CDK1 and PLK1 activation. *Mol*
813 *Cell* 71(1):117-128.
814 Levasseur M, Dumollard R, Chambon JP, Hebras C, Sinclair M, Whitaker M, McDougall A. 2013.
815 Release from meiotic arrest in ascidian eggs requires the activity of two phosphatases but not
816 camkii. *Development* 140(22):4583-4593.
817 Levasseur M, McDougall A. 2000. Sperm-induced calcium oscillations at fertilisation in ascidians
818 are controlled by cyclin B1-dependent kinase activity. *Development* 127(3):631-641.
819 Levasseur MD, Thomas C, Davies OR, Higgins JMG, Madgwick S. 2019. Aneuploidy in oocytes is
820 prevented by sustained Cdk1 activity through degron masking in cyclin B1. *Dev Cell* 48(5):672-
821 684.
822 Levine K, Kiang L, Jacobson MD, Fisher RP, Cross FR. 1999. Directed evolution to bypass cyclin
823 requirements for the Cdc28p cyclin-dependent kinase. *Mol Cell* 4(3):353-363.
824 Lobon CM, Acuna JL, Lopez-Alvarez M, Capitanio FL. 2011. Heritability of morphological and
825 life history traits in a pelagic tunicate. *Mar Ecol Prog Ser*. 422:145-154.
826 Macneill SA, Nurse P. 1993. Mutational analysis of the fission yeast p34cdc2 protein-kinase gene.
827 *Mol Gen Genet.* 236(2-3):415-426.
828 Nakanishi M, Katsuno Y, Niida H, Murakami H, Shimada M. 2010. Chk1-cyclin A/Cdk1 axis
829 regulates origin firing programs in mammals. *Chromosome Res*. 18(1):103-113.
830 Naville M, Henriet S, Warren I, Sumic S, Reeve M, Volff JN, Chourrout D. 2019. Massive changes
831 of genome size driven by expansions of non-autonomous transposable elements. *Curr Biol*.
832 29(7):1161-1168.
833 Nolen B, Taylor S, Ghosh G. 2004. Regulation of protein kinases: Controlling activity through
834 activation segment conformation. *Mol Cell* 15(5):661-675.
835 Nowack MK, Harashima H, Dissmeyer N, Zhao XA, Bouyer D, Weimer AK, De Winter F, Yang
836 F, Schnittger A. 2012. Genetic framework of cyclin-dependent kinase function in arabidopsis.
837 *Dev Cell* 22(5):1030-1040.

838 Okano-Uchida T, Sekiai T, Lee KS, Okumura E, Tachibana K, Kishimoto T. 1998. In vivo
839 regulation of cyclin A/Cdc2 and cyclin B/Cdc2 through meiotic and early cleavage cycles in
840 starfish. *Dev Biol.* 197(1):39-53.
841 Ord M, Loog M. 2019. How the cell cycle clock ticks. Mol Biol Cell. 30(2):169-172.
842 Ord M, Moll K, Agerova A, Kivi R, Faustova I, Venta R, Valk E, Loog M. 2019a. Multisite
843 phosphorylation code of Cdk. *Nat Struct Mol Biol.* 26(7):649-658.
844 Ord M, Venta R, Moll K, Valk E, Loog M. 2019b. Cyclin-specific docking mechanisms reveal the
845 complexity of M-Cdk function in the cell cycle. *Mol Cell*. 75(1):76-89.
846 Ovrebo JI, Campsteijn C, Kourtesis I, Hausen H, Raasholm M, Thompson EM. 2015. Functional
847 specialization of chordate Cdk1 paralogs during oogenic meiosis. *Cell Cycle* 14(6):880-893.
848 Rogozin IB, Belinky F, Pavlenko V, Shabalina SA, Kristensen DM, Koonin EV. 2016.
849 Evolutionary switches between two serine codon sets are driven by selection. *Proc Natl Acad*
850 *Sci U S A.* 113(46):13109-13113.
851 Santamaria D, Barriere C, Cerqueira A, Hunt S, Tardy C, Newton K, Caceres JF, Dubus P,
852 Malumbres M, Barbacid M. 2007. Cdk1 is sufficient to drive the mammalian cell cycle. *Nature*
853 448(7155):811-U818.
854 Schaffner SF. 2004. The x chromosome in population genetics. Nat Rev Genet. 5(1):43-51.
855 Seller CA, O'Farrell PH. 2018. Rif1 prolongs the embryonic s phase at the *Drosophila* mid-blastula
856 transition. *Plos Biol.* 16(5).
857 Sonnhammer ELL, Koonin EV. 2002. Orthology, paralogy and proposed classification for paralog
858 subtypes. *Trends Genet*. 18(12):619-620.
859 Staver JM, Strathmann RR. 2002. Evolution of fast development of planktonic embryos to early
860 swimming. *Biol Bull.* 203(1):58-69.
861 Strathmann RR, Staver JM, Hoffman JR. 2002. Risk and the evolution of cell-cycle durations of
862 embryos. *Evolution* 56(4):708-720.
863 Swaffer MP, Jones AW, Flynn HR, Snijders AP, Nurse P. 2016. Cdk substrate phosphorylation and
864 ordering the cell cycle. *Cell* 167(7):1750-1761.
865 Szmyd R, Niska-Blakie J, Diril MK, Nunes PR, Tzelepis K, Lacroix A, van Hul N, Deng LW,
866 Matos J, Dreesen O et al. 2019. Premature activation of Cdk1 leads to mitotic events in s phase
867 and embryonic lethality. *Oncogene* 38(7):998-1018.
868 Troedsson C, Bouquet JM, Aksnes DL, Thompson EM. 2002. Resource allocation between somatic
869 growth and reproductive output in the pelagic chordate *Oikopleura dioica* allows opportunistic
870 response to nutritional variation. *Mar Ecol Prog Ser*. 243(11):83-91.
871 Tsai TYC, Theriot JA, Ferrell JE. 2014. Changes in oscillatory dynamics in the cell cycle of early
872 *Xenopus laevis* embryos. *Plos Biol.* 12(2):e1001788.
873 van der Voet M, Lorson MA, Srinivasan DG, Bennett KL, van den Heuvel S. 2009. *C. elegans*
874 mitotic cyclins have distinct as well as overlapping functions in chromosome segregation. *Cell*
875 *Cycle* 8(24):4091-4102.
876 Wood DJ, Korolchuk S, Tatum NJ, Wang LZ, Endicott JA, Noble MEM, Martin MP. 2019.
877 Differences in the conformational energy landscape of CDK1 and CDK2 suggest a mechanism
878 for achieving selective CDK inhibition. *Cell Chem Biol.* 26(1):121-130.
879 Yang ZH. 2007. Paml 4: Phylogenetic analysis by maximum likelihood. *Mol Biol Evol*.
880 24(8):1586-1591.
881 Yuan K, Seller CA, Shermoen AW, O'Farrell PH. 2016. Timing the *Drosophila* mid-blastula
882 transition: A cell cycle-centerec view. *Trends Genet*. 32(8):496-507.
883 Zhang JZ, Rosenberg HF, Nei M. 1998. Positive darwinian selection after gene duplication in
884 primate ribonuclease genes. *Proc Natl Acad Sci USA.* 95(7):3708-3713.

Figure 1

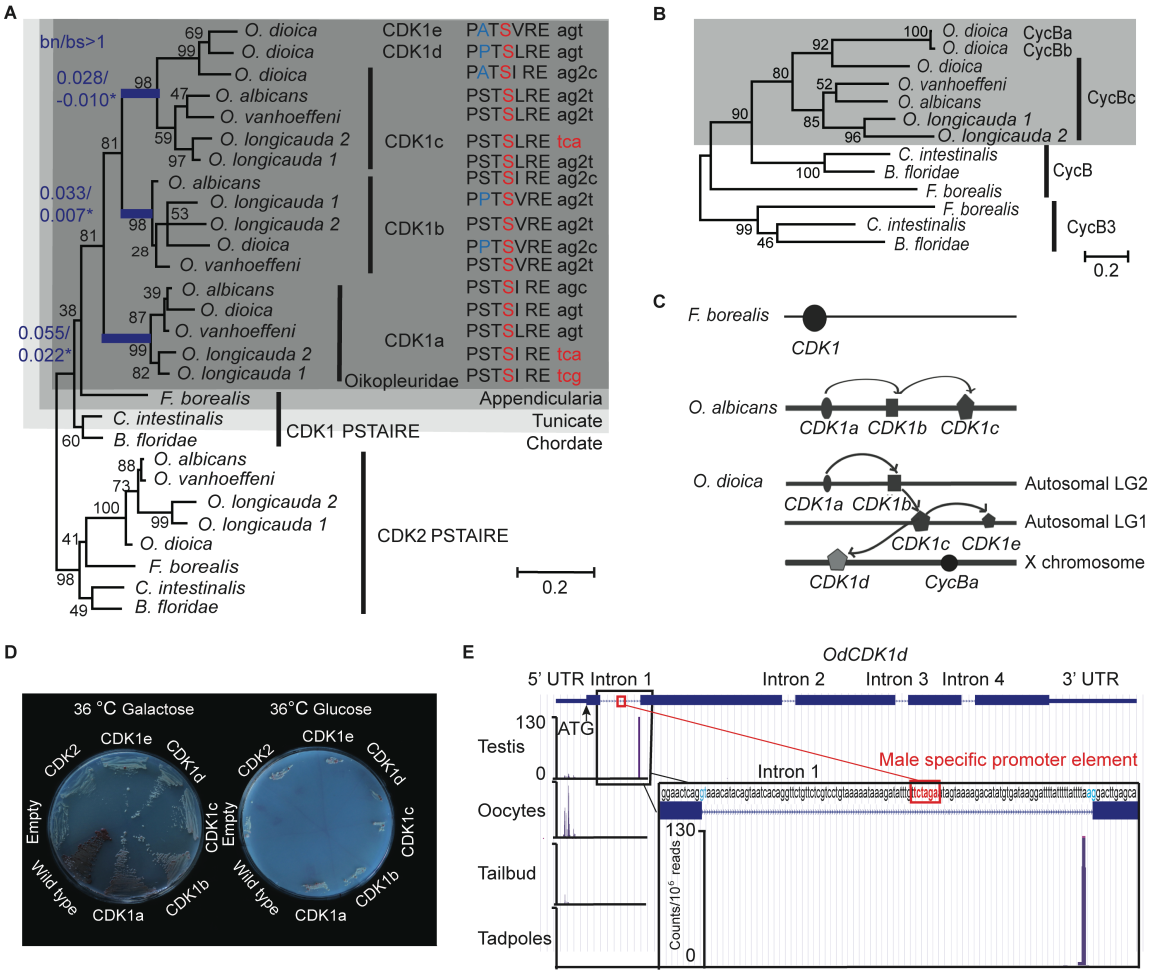

Figure 2

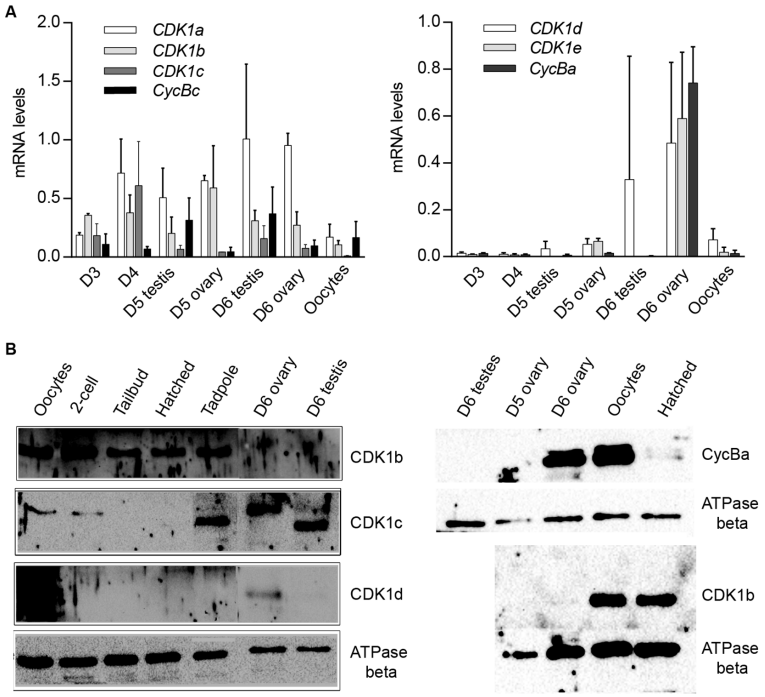

Figure 3

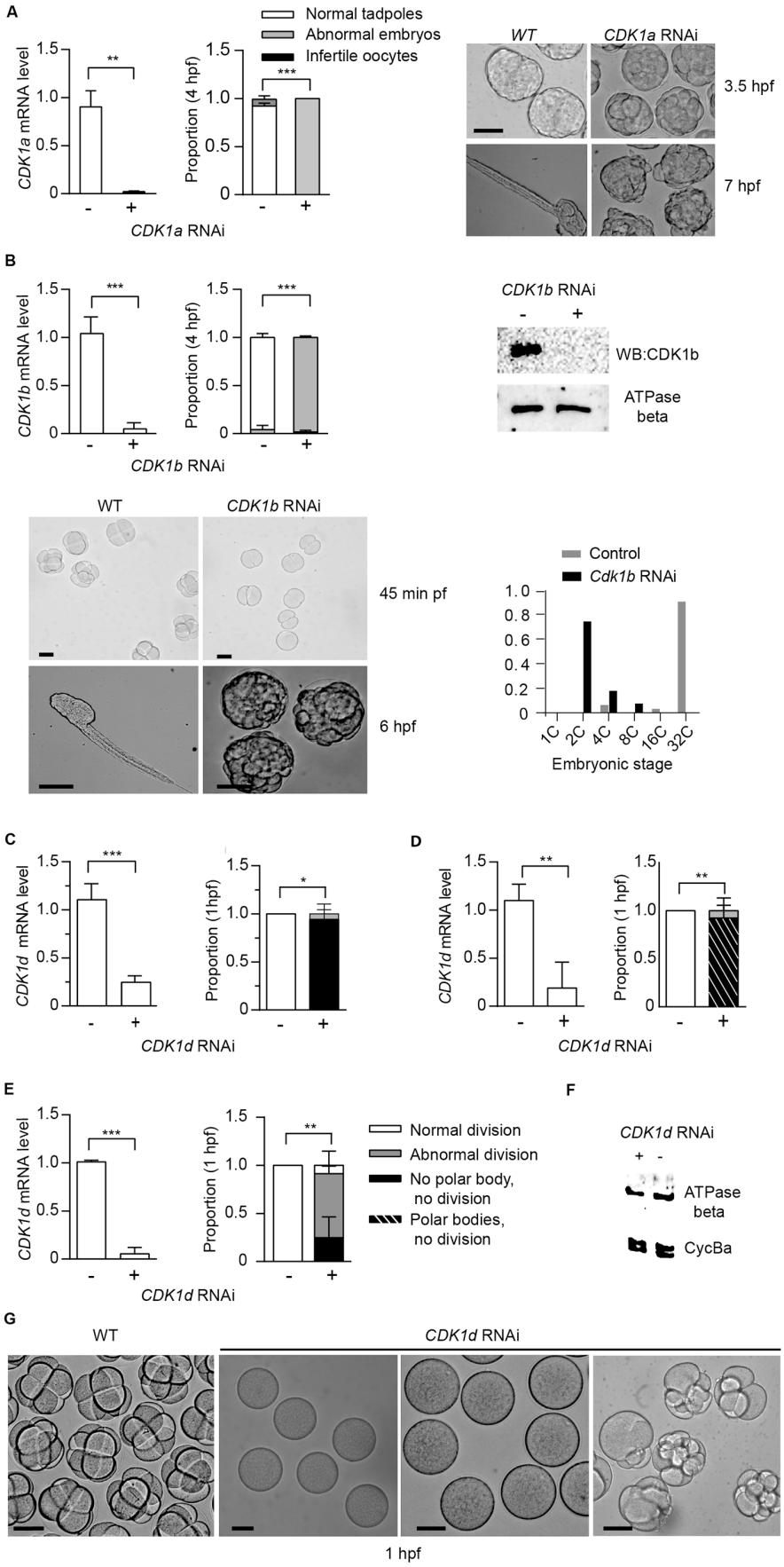
A
Normal tadpoles
Abnormal embryos
Infertile oocytes
CDK1a mRNA level
Proportion (4 hpf)
CDK1a RNAi
WT
CDK1a RNAi
3.5 hpf
7 hpf
B
CDK1b mRNA level
Proportion (4 hpf)
CDK1b RNAi
WB:CDK1b
ATPase beta
WT
CDK1b RNAi
45 min pf
6 hpf
Control
Cdk1b RNAi
Embryonic stage
1C
2C
4C
8C
16C
32C
C
CDK1d mRNA level
Proportion (1hpf)
CDK1d RNAi
D
CDK1d mRNA level
Proportion (1 hpf)
CDK1d RNAi
E
CDK1d mRNA level
Proportion (1 hpf)
CDK1d RNAi
Normal division
Abnormal division
No polar body, no division
Polar bodies, no division
F
CDK1d RNAi
ATPase beta
CycBa
G
WT
CDK1d RNAi
1 hpf

Figure 4

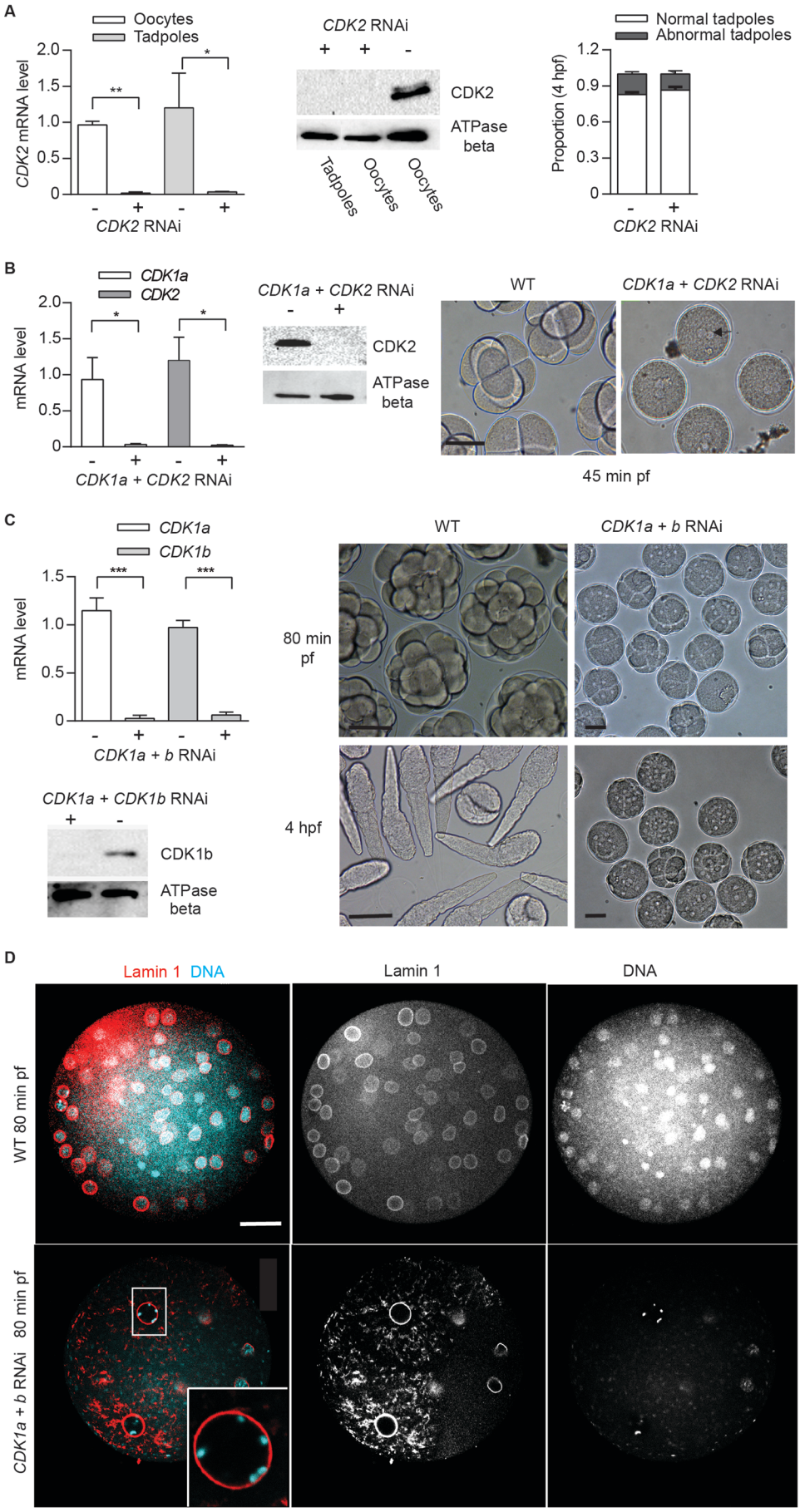
A
Oocytes
Tadpoles
CDK2 mRNA level
2.0
1.5
1.0
0.5
0
**
*
- + - +
CDK2 RNAi
CDK2 RNAi
+ + -
CDK2
ATPase beta
Tadpoles
Oocytes
Oocytes
Normal tadpoles
Abnormal tadpoles
Proportion (4 hpf)
1.2
0.9
0.6
0.3
0
- +
CDK2 RNAi
B
CDK1a
CDK2
mRNA level
2.0
1.5
1.0
0.5
0
*
*
- + - +
CDK1a + CDK2 RNAi
CDK1a + CDK2 RNAi
- +
CDK2
ATPase beta
WT
CDK1a + CDK2 RNAi
45 min pf
C
CDK1a
CDK1b
mRNA level
1.5
1.0
0.5
0
***
***
- + - +
CDK1a + b RNAi
CDK1a + CDK1b RNAi
+ -
CDK1b
ATPase beta
WT
CDK1a + b RNAi
80 min pf
4 hpf
D
Lamin 1 DNA
Lamin 1
DNA
WT 80 min pf
CDK1a + b RNAi 80 min pf

Figure 5

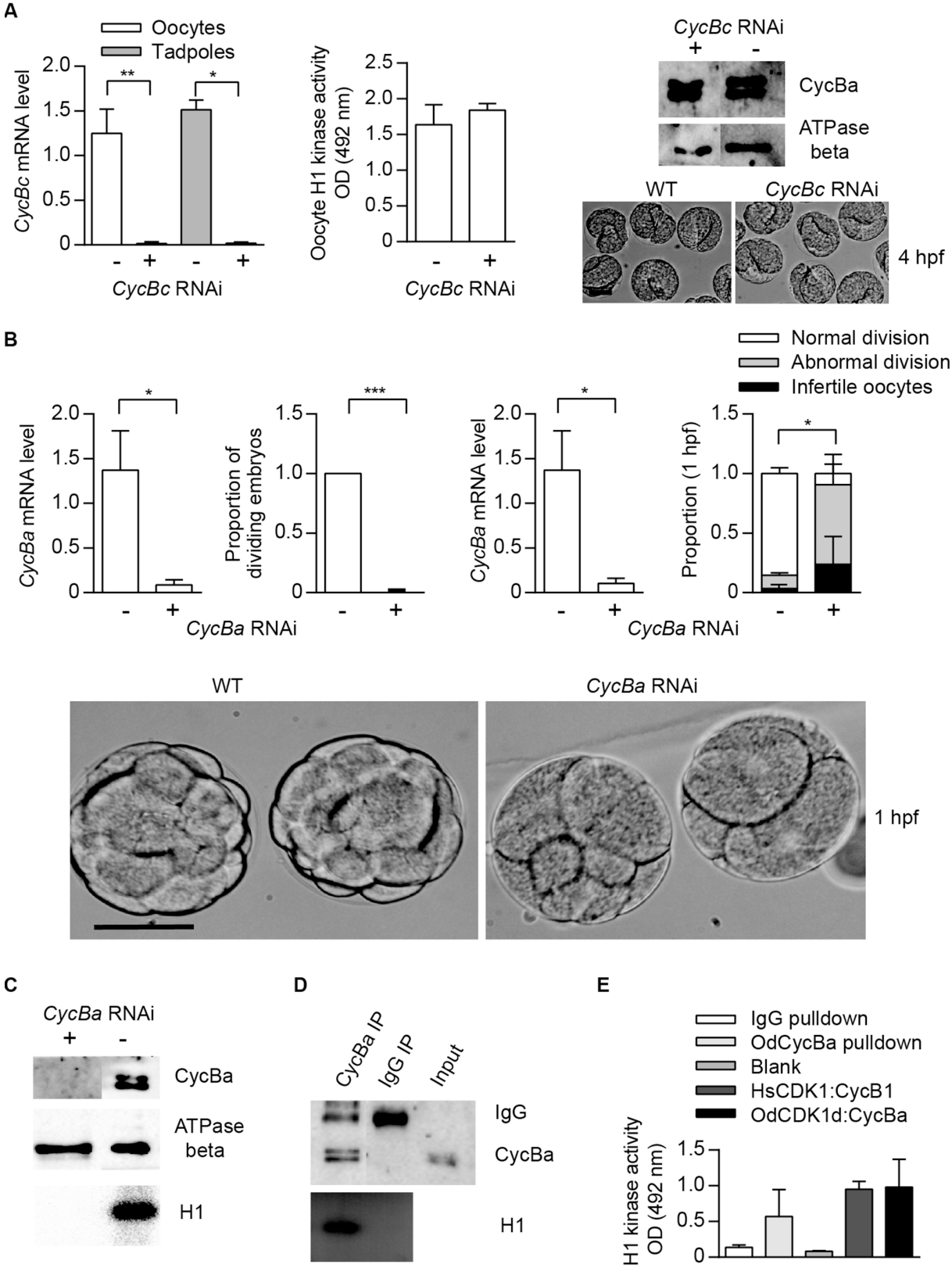
A
Oocytes
Tadpoles
CycBc mRNA level
2.0
1.5
1.0
0.5
0
**
*
- + - +
CycBc RNAi
Oocyte H1 kinase activity OD (492 nm)
2.5
2.0
1.5
1.0
0.5
0
- +
CycBc RNAi
CycBc RNAi
+ -
CycBa
ATPase beta
WT
CycBc RNAi
4 hpf
B
Normal division
Abnormal division
Infertile oocytes
CycBa mRNA level
*
- +
CycBa RNAi
Proportion of dividing embryos
***
- +
CycBa mRNA level
*
- +
CycBa RNAi
Proportion (1 hpf)
*
- +
WT
CycBa RNAi
1 hpf
C
CycBa RNAi
+ -
CycBa
ATPase beta
H1
D
CycBa IP
IgG IP
Input
IgG
CycBa
H1
E
IgG pulldown
OdCycBa pulldown
Blank
HsCDK1:CycB1
OdCDK1d:CycBa
H1 kinase activity OD (492 nm)
1.5
1.0
0.5
0

Figure 6

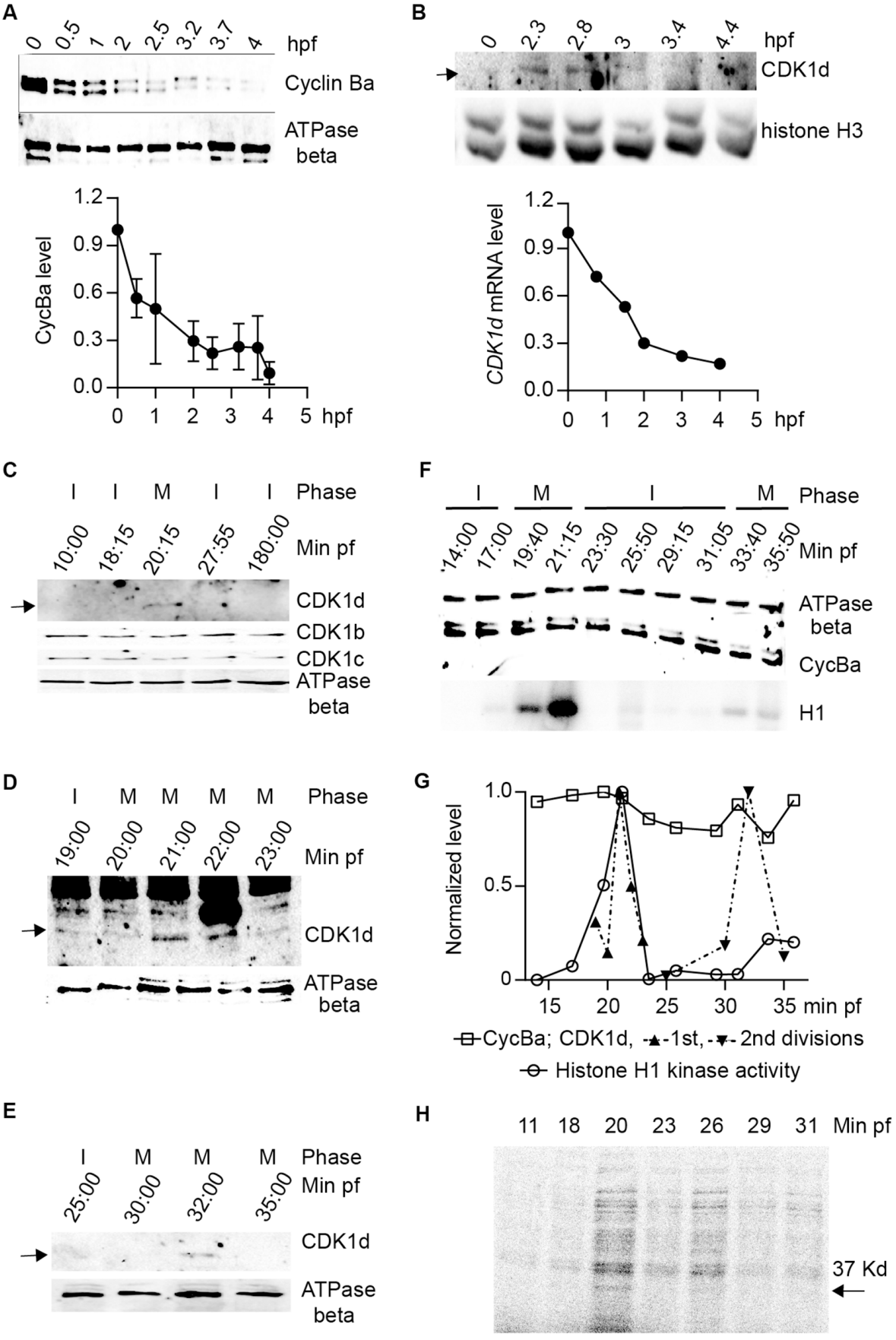
A
0 0.5 1 2 2.5 3.2 3.7 4 hpf
Cyclin Ba
ATPase beta
CycBa level
1.2 0.9 0.6 0.3 0.0
0 1 2 3 4 5 hpf
B
0 2.3 2.8 3 3.4 4.4 hpf
CDK1d
histone H3
CDK1d mRNA level
1.2 0.9 0.6 0.3 0.0
0 1 2 3 4 5 hpf
C
I I M I I Phase
10:00 18:15 20:15 27:55 180:00 Min pf
CDK1d
CDK1b
CDK1c
ATPase beta
F
I M I M Phase
14:00 17:00 19:40 21:15 23:30 25:50 29:15 31:05 33:40 35:50 Min pf
ATPase beta
CycBa
H1
D
I M M M M Phase
19:00 20:00 21:00 22:00 23:00 Min pf
CDK1d
ATPase beta
G
Normalized level
1.0 0.5 0
15 20 25 30 35 min pf
CycBa; CDK1d, 1st, 2nd divisions
Histone H1 kinase activity
E
I M M M Phase
25:00 30:00 32:00 35:00 Min pf
CDK1d
ATPase beta
H
11 18 20 23 26 29 31 Min pf
37 Kd

Figure 7

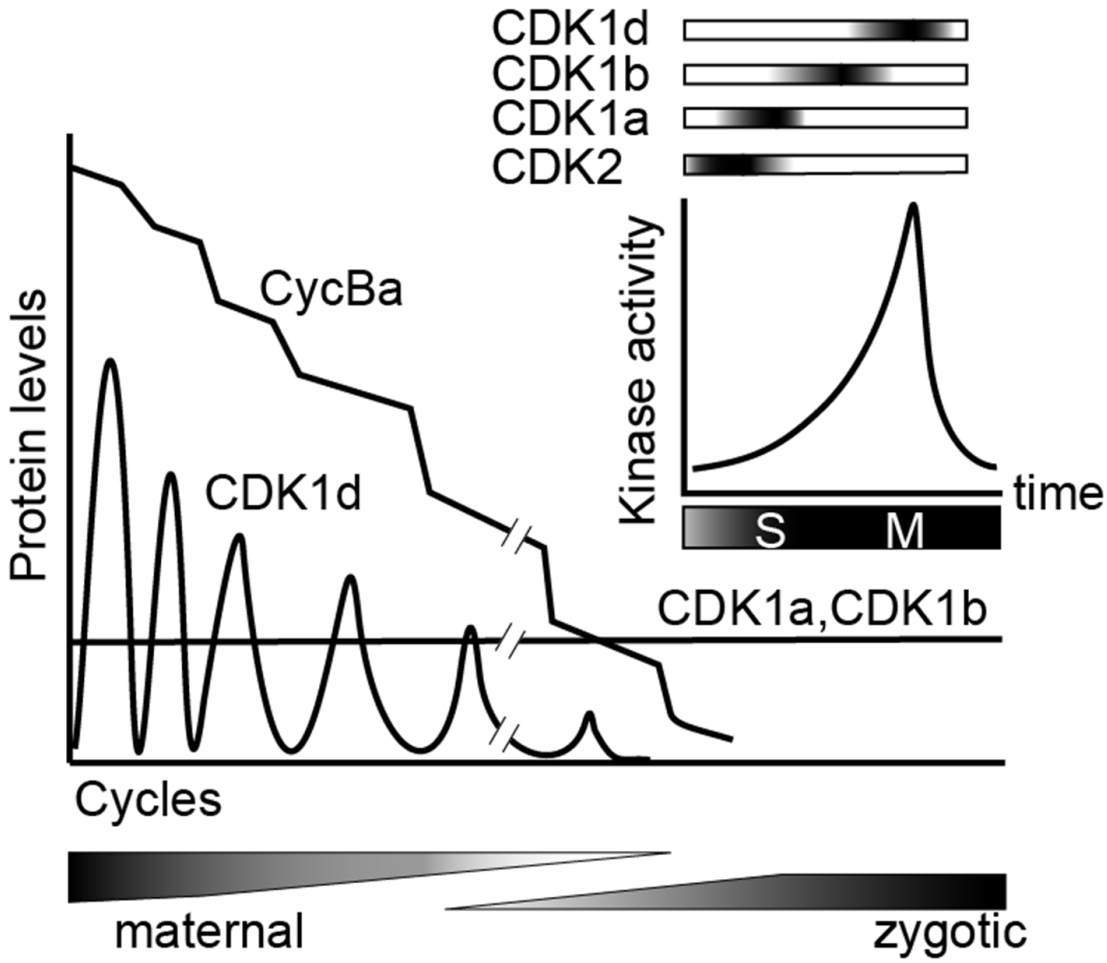
CDK1d
CDK1b
CDK1a
CDK2
Kinase activity
time
S
M
Protein levels
CycBa
CDK1d
CDK1a,CDK1b
Cycles
maternal
zygotic